



**REDUNDANT WAVELET-BASED IMAGE
RESTORATION USING A PRIORI
INFORMATION**

THESIS

Mary Kristin Marcum, 2nd Lieutenant, USAF

AFIT/GE/ENG/01M-17

**DEPARTMENT OF THE AIR FORCE
AIR UNIVERSITY**

AIR FORCE INSTITUTE OF TECHNOLOGY

Wright-Patterson Air Force Base, Ohio

APPROVED FOR PUBLIC RELEASE; DISTRIBUTION UNLIMITED.

20010706 125

The views expressed in this thesis are those of the author and do not reflect the official policy or position of the United States Air Force, Department of Defense, or the U. S. Government.

AFIT/GE/ENG/01M-17

REDUNDANT WAVELET-BASED IMAGE RESTORATION USING A PRIORI
INFORMATION

THESIS

Presented to the Faculty

Department of Computer and Electrical Engineering

Graduate School of Engineering and Management

Air Force Institute of Technology

Air University

Air Education and Training Command

In Partial Fulfillment of the Requirements for the

Degree of Master of Science in Engineering and Environmental Management

Mary Kristin Marcum, B.S.

2nd Lieutenant, USAF

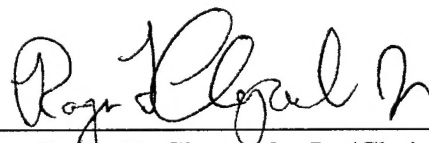
March 2001

APPROVED FOR PUBLIC RELEASE; DISTRIBUTION UNLIMITED.

REDUNDANT WAVELET-BASED IMAGE RESTORATION USING A PRIORI
INFORMATION

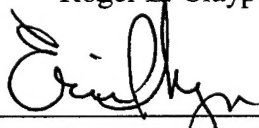
Mary Kristin Marcum, B.S.
2nd Lieutenant, USAF

Approved:



Roger L. Claypoole, Jr. (Chairman)

8 MAR 01
date



Eric P. Magee (Member)

8 MAR 01
date



Mark E. Oxley (Member)

8 Mar 01
date

Acknowledgments

I would like to express my sincere appreciation to my faculty advisor, Maj. Roger Claypoole, for his guidance, support and encouragement throughout this thesis effort. His insight and experience was certainly appreciated. I would, also, like to thank my committee members, Maj. Eric Magee and Dr. Mark Oxley, for both their support and assistance provided to me in this endeavor.

I am indebted to many friends and colleagues who provided support in various ways throughout my time here, a special thanks to them all. I also want to thank my family and friends in Tennessee especially my mother, father and sisters for their continual encouragement and support even though they were far away. Last but not least, I want to thank my children for being so wonderful, patient and encouraging during this very busy year and a half.

Mary Kristin Marcum

Table of Contents

	Page
Acknowledgments	iv
List of Figures	vii
List of Tables	x
Abstract	xi
I. Introduction	1
Background	1
Problem	1
Summary of Current Knowledge	2
Assumptions	4
Scope	4
Standard	5
Approach	5
II. Background	6
Wavelets	7
Denoising	11
Redundant Wavelets and Denoising	14
Other Wavelet-Based Techniques	15
Adaptive Wavelet Transforms Via Lifting	15
Summary	17
III. Methodology	18
Lifting	18
Wavelet Polyphase Representation	23
Redundancy	28
Adaptivity	29
Denoising/Thresholding	30
IV. Results	32
Error Measures	32
Denoising Experiments	33

Denoising Results.....	34
Summary	62
 V. Conclusion.....	 63
Applications	63
Recommendations for Future Research	64
 Bibliography.....	 65
Vita	67

List of Figures

Figure	Page
2.1. Filterbank Implementation of Discrete Wavelet Transform	10
3.1. Forward Lifting Stage	20
3.2. Inverse Lifting Stage	20
3.3. Prediction Design	21
3.4. Update Design	23
3.5. Polyphase Form of Wavelet Transform	24
3.6. Lifting operations in Polyphase Form	25
3.7. Combination of Lifting Steps in Polyphase Form	25
3.8. Redundant Lifting Scheme	28
4.1. Original star image before the addition of noise	36
4.2. Training star image used for adapting the transform	37
4.3. Star image and additive Gaussian noise(high noise)	38
4.4. Star image denoised using (4,4) lift, 4 vanishing moments (non-adaptive) and... a soft threshold equal to 3 times the standard deviation of the noise(high noise)	39
4.5. Star image denoised using (4,4) lift, 2 vanishing moments, adaptive to noisy signal and a soft threshold equal to 3 times the standard deviation of the..... noise(high noise)	40
4.6. Star image denoised using (4,4) lift, 2 vanishing moments, adaptive to training . signal and a soft threshold equal to 1.5 times the adaptive threshold set by the... transform(high noise)	41
4.7. Star image denoised using (4,4) lift, 2 vanishing moments, adaptive to training . signal and a soft threshold equal to 3 times the standard deviation of the..... noise(high noise).	42

4.8. Star image denoised using (4,4) lift, 4 vanishing moments (non-adaptive)..... and a hard threshold equal to 3.6 times the standard deviation of the noise(high noise)	43
4.9 Star image denoised using (4,4) lift, 2 vanishing moments, adaptive to..... noisy signal and a hard threshold equal to 3.6 times the standard deviation of the noise(high noise)	44
4.10. Star image denoised using (4,4) lift, 2 vanishing moments, adaptive to training signal and a hard threshold equal to 3 times the adaptive threshold..... set by the transform(high noise)	45
4.11. Star image denoised using (4,4) lift, 2 vanishing moments, adaptive to training signal and a hard threshold equal to 3.6 times the standard deviation.... of the noise(high noise)	46
4.12. Star image and additive Gaussian noise(medium noise)	51
4.13. Star image denoised using (4,4) lift, 4 vanishing moments (non-adaptive) and.. a soft threshold equal to 3 times the standard deviation of the noise(medium noise)	52
4.14. Star image denoised using (4,4) lift, 2 vanishing moments, adaptive to noisy.... signal and a soft threshold equal to 3 times the standard deviation of the..... noise(medium noise)	53
4.15. Star image denoised using (4,4) lift, 2 vanishing moments, adaptive to training signal and a soft threshold equal to 1.5 times the adaptive threshold set by the... transform(medium noise)	54
4.16. Star image denoised using (4,4) lift, 2 vanishing moments, adaptive to training signal and a soft threshold equal to 3 times the standard deviation of the..... noise(medium noise).	55
4.17. Star image denoised using (4,4) lift, 4 vanishing moments (non-adaptive)..... and a hard threshold equal to 3.6 times the standard deviation of the noise (medium noise)	56
4.18 Star image denoised using (4,4) lift, 2 vanishing moments, adaptive to..... noisy signal and a hard threshold equal to 3.6 times the standard deviation of the noise(medium noise)	57
4.19. Star image denoised using (4,4) lift, 2 vanishing moments, adaptive to training signal and a hard threshold equal to 3 times the adaptive threshold..... set by the transform(medium noise)	58

4.20. Star image denoised using (4,4) lift, 2 vanishing moments, adaptive to training signal and a hard threshold equal to 3.6 times the standard deviation.... of the noise(medium noise).....	59
---	----

List of Tables

Table	Page
4.1. Error measurements for whole star image using a soft threshold	47
4.2. Error measurements for training area of star image using a soft threshold.....	48
4.3. Error measurements for whole star image using a hard threshold	60
4.4. Error measurements for training area of star image using a hard threshold	61

Abstract

Reconnaissance missions and satellites collect hundreds of images loaded with valuable information to be utilized by the Air Force. Intelligence operations must analyze these images to extract the information needed to help commanders make important decisions. No matter how obtained, images of this type are often degraded by noise due to disruptions such as atmospheric disturbances, optical system variations, motion, and large distance from the sensor to the source. This noise must be removed effectively to improve the quality of these images and ensure that the information contained in them can be correctly extracted. The Air Force relies on the critical information contained in these images and therefore effective noise removal is critical.

Limitations in current image restoration techniques cause visually disturbing effects in reconstructed images. Therefore, a more effective algorithm for noise removal is required. This thesis will explore the use of redundant wavelet-based multiresolution image processing and a priori information to enhance current image restoration techniques. Often on an airplane, tank or other military vehicle or building there may be a known symbol, which can be used as perfect a priori information to restore the entire image. An adaptive redundant discrete wavelet transform will be trained using this a priori information. Constant and adaptive thresholds are used on the noisy image while in the wavelet domain. The quality of the reconstructed image is improved over non-adaptive techniques.

REDUNDANT WAVELET-BASED IMAGE RESTORATION USING A PRIORI INFORMATION

I. Introduction

1.1 Background

Reconnaissance missions and satellites collect hundreds of images loaded with valuable information to be utilized by the Air Force. Intelligence operations must analyze these images to extract the information needed to help commanders make important decisions. No matter how obtained, images of this type are often degraded by noise due to disruptions such as atmospheric disturbances, optical system variations, motion, and large distance from the sensor to the source. This noise must be removed effectively to improve the quality of these images and ensure that the information contained in them can be correctly extracted. The Air Force relies on the critical information contained in these images and therefore effective noise removal is critical.

1.2 Problem

Image restoration attempts to recover an image which has been degraded. This thesis will explore the use of redundant wavelet-based multiresolution image processing and a priori information to enhance current image restoration techniques. Perfect a priori information about an object in an image will be assumed. Often on an airplane, tank or other military vehicle or building there may be a known symbol, which can be used as

perfect a priori information to restore the entire image. An adaptive redundant discrete wavelet transform will be trained using this a priori information. Then the new adapted wavelet will be used to transform an image in which the object should appear. Wavelets will be used because they have proven useful in many signal and image processing techniques. Wavelet decompositions provide efficient representations for a wide range of signals. While in the wavelet domain, the soft or hard-threshold techniques [2] will be used to remove noise. Then the image is transformed back into the image space and the area of the image containing the object of interest should be improved. A successful algorithm accomplishing improved restoration of an image, which contains the training object, could be of great value to the Air Force in image analysis operations.

1.3 Summary of Current Knowledge

Many techniques for image restoration have been developed and studied extensively. Even with these many image restoration techniques available, research continues in this area due to limitations with each of these techniques. Many of these limitations cause restored imagery to have visually disturbing effects.

For example, many techniques degrade edges. Edges in an image provide important object definition but are difficult to deal with in image restoration because of their high frequency content. The corruption of high frequencies causes blurring at these edge locations in an image. Another problem occurring at the location of edges is the Gibbs phenomenon, an interchange of overshooting and undershooting a target level. This phenomenon is associated with many current signal and image processing

techniques. Thus, researchers continually attempt to develop improved image restoration techniques.

One way researchers work to solve these problems is with adaptive wavelet transforms. Adaptive transforms use some or all of the transform parameters to adapt to the signal, typically to minimize some error criterion. The lifting construction [9, 10, 11] developed to implement the wavelet multiresolution transform provides an easy way to introduce adaptivity using prediction error energy as a metric. Adaptable wavelet transforms have been developed using the lifting construction [6] and show promise in the search for high quality image restoration.

A different approach to image restoration was used in [3] by using a priori information about an image. Perfect knowledge of a portion of the image was assumed and was used to help remove noise from the entire image in the Fourier transform domain. That research showed that repeated use of this information to restore the image using a Fourier transform technique improved the degraded image in only the opposite quadrant of the perfect information. Other quadrants in the image experienced minimal improvement. To achieve these results, the perfect information had to be repeatedly placed into the image and then the algorithm was run to reduce noise. The noise reduction outside the area of perfect knowledge depends upon the noise correlation properties [3]. For this technique, 25% of the image needs to be perfectly known and often knowing this much a priori information about the image is unrealistic.

1.4 Assumptions

In this thesis, perfect knowledge of an object in a digital image will be known. Also the relative size and rotation of this object in the image must be known. This information is necessary for development at this stage due to the fact that the transforms used will not be scale or rotation invariant. However, due to the shift invariant nature of the proposed algorithms, the relative position of the object can freely vary. Images will be degraded with additive Gaussian zero mean white noise. No multiplicative noise will be introduced into the image model.

1.5 Scope

The research will begin by having complete knowledge of an object in an image. The orientation, size and intensity of the object will be known. The adaptive wavelet transform will be trained using this information; this transform will then be used for image restoration. Comparisons will be made between these images using soft-threshold noise removal and hard-threshold noise removal [2]. Non-adaptive techniques will be run so that comparisons may be made. The transforms used will be shift-invariant so that knowledge of the location will not be necessary; this redundancy will also reduce the pseudo-Gibbs phenomenon associated with the non-redundant discrete wavelet transform-based restoration techniques.

1.6 Standards

Images will be evaluated using mean square error and L^∞ error criteria between the original image before noise is added and the image after noise removal. This evaluation will be done for the entire image and also locally on the object of interest. More importantly, the visual appearance of the images will be compared to other image restoration techniques to determine which is more appealing.

1.7 Approach

The multiresolution transforms via lifting developed by Claypoole [6] will be modified to complete this research. The transforms will be trained using the known information of a local area or object. Then, the trained transforms will be used to process an entire image containing the training information with degradations. All simulations will be performed in MATLAB®.

II. Background

In its most general form, image restoration is any technique to recover an image that has been degraded. Whether captured by camera, x-ray, or other optical systems, images are typically degraded by various phenomena. Movement of the camera or other external disruptions can cause blur in a photographic image, which is visually disturbing. In digital imaging, other forms of interference degrade the image. In the transmission of a digital image, interference and thermal noise can cause degradation throughout the image. This noise in an image is purely an artifact of the image process; one goal of image restoration is to remove that noise.

Wavelets have become an important tool for many image-processing techniques. They provide an efficient representation for a broad range of signals. In addition to this parsimonious representation, they provide spatial and frequency localization, which helps to reduce the Gibbs phenomenon to only a local effect hence referred to as pseudo-Gibbs phenomenon [5]. The lifting approach to wavelets provides an easy implementation and a way to introduce adaptivity. Redundancy provides a better representation by allowing for any shift in the data while averaging out most of the pseudo-Gibbs phenomenon and other restoration artifacts. This thesis will explore the use of these redundant and adaptive multiresolution image-processing techniques and a priori information to enhance current image restoration processing techniques.

2.1 Wavelets

Many techniques for image restoration have been developed and studied extensively. Effective algorithms for removing degradation exist in the frequency domain. Mathematical models for image restoration are also available. More recently, wavelet-based image restoration techniques have proven to be very effective. The wavelet decomposition is useful because signal information is contained in a few coefficients. Another valuable feature of the wavelet decomposition is the fact that the coefficients simultaneously provide information on time/location and frequency. Wavelet techniques preserve smooth areas, polynomials and even piecewise polynomials very well but have trouble maintaining clear, sharp edges.

The successive projection of a function f into smaller orthogonal subspaces is a primary focus of wavelet multiresolution analysis. Shifts and dilations of a low-pass scaling function $\phi(t)$ and a band pass wavelet function $\psi(t)$ form the smaller subspaces. Presented below is a derivation of the multiresolution analysis for orthogonal wavelets.

Let $\{V_m\}_{m \in \mathbb{Z}}$ be a sequence of nested subspaces in $L^2(\mathbb{R})$ and $V_m \subset V_{m-1} \quad \forall m \in \mathbb{Z}$ is required. Now let f be a function in the subspace V_{m-1} for some m . The function $f \in V_{m-1}$ is projected into the nested subspace $V_m \subset V_{m-1}$ by a projection operator P_m . This projection operator P_m eliminates the part of f which is not in V_m , while the portion of f in V_m remains undisturbed. The orthogonal projection operator, $Q_m = I - P_m$, projects the function f into the subspace $W_m \subset V_{m-1}$. Here, I is the identity operator. Q_m and P_m are orthogonal; therefore, $P_m Q_m = Q_m P_m = 0$.

Let $\{W_m\}_{m \in \mathbb{Z}}$ be another sequence of nested subspaces where $W_m \subset W_{m-1} \quad \forall m \in \mathbb{Z}$. Let the span of $V_m \cup W_m = V_{m-1}$ and let V_m and W_m be orthogonal subspaces (i.e., $V_{m-1} = V_m \oplus W_m$ and $V_m \cap W_m = \emptyset$).

Let the set of scaling functions $\{\phi_{m,l}\}_{l \in \mathbb{Z}}$ be an orthonormal basis for V_m and let the set of wavelet functions $\{\psi_{m,l}\}_{l \in \mathbb{Z}}$ be an orthonormal basis for W_m . $V_m \subset V_{m-1}$, and therefore, $\phi_{m,l}$ can be expanded in terms of $\phi_{m-1,k}$ as:

$$\phi_{m,l}(x) = \sum_k c_{m-1,l}(k) \phi_{m-1,k}(x). \quad (2.1)$$

Take the inner product of $\phi_{m,l}$ with the basis function $\phi_{m-1,k}$ to determine the value of the coefficient $c_{m-1,l}(k)$ as follows:

$$\langle \phi_{m,l}, \phi_{m-1,k} \rangle = \int_{-\infty}^{\infty} \phi_{m,l}(x) \phi_{m-1,k}(x) dx. \quad (2.2)$$

If $h_{l,k} = \langle \phi_{m,l}, \phi_{m-1,k} \rangle$, then the new expansion of $\phi_{m,l}$ becomes:

$$\phi_{m,l}(x) = \sum_k h_{m-1,l,k} \phi_{m-1,k}(x). \quad (2.3)$$

Now to form an orthogonal wavelet transform, the set of functions $\phi_{m,l}$ must satisfy Equation (2.3) for all m . For a discrete wavelet transform, each $\phi_{m,l}$ must be created from integer shifts and dyadic dilations (l and 2^m , respectively) of the scaling function $\phi(x)$. Therefore, Equation (2.3) can be written as:

$$\phi(x-l) = \sum_k h(k-2l) \phi(2x-k). \quad (2.4)$$

Let $g(k-2l) = \langle \psi_{m,l}, \phi_{m-1,k} \rangle$ and the wavelet equation can be written as:

$$\psi(x-l) = \sum_k g(k-2l) \phi(2x-k). \quad (2.5)$$

Together, Equations (2.4) and (2.5) create the *wavelet recursion relations* [8].

The function f can be completely described as a linear combination of the basis functions in the subspace V_{m-1} . The projection of f into the subspace V_m can be described in terms of the basis functions for V_m . In a similar way, the projection of f into the subspace W_m can be described in terms of the basis functions for W_m . These projections are:

$$\begin{aligned} [P_m f](x) &= \sum_l c_{m,l} \phi_{m,l}(x), \\ [Q_m f](x) &= \sum_l d_{m,l} \psi_{m,l}(x), \end{aligned}$$

where $c_{m,l} = \langle P_m f, \phi_{m,l} \rangle$ and $d_{m,l} = \langle Q_m f, \psi_{m,l} \rangle$. The function f can be written as

$$f = P_m f + Q_m f \quad (2.6)$$

because $P + Q = \mathbf{I}$. Any given decomposition coefficient in V_m can be written as:

$$\begin{aligned} c_{m,l} &= \langle P_m f, \phi_{m,l} \rangle \\ &= \langle (f - Q_m f), \phi_{m,l} \rangle \\ &= \langle f, \phi_{m,l} \rangle - \langle Q_m f, \phi_{m,l} \rangle \\ &= \langle f, \phi_{m,l} \rangle. \end{aligned} \quad (2.7)$$

Expand f in terms of the basis functions in V_{m-1} and substitute the results into Equation (2.7) yielding

$$\begin{aligned} c_{m,l} &= \left\langle \left(\sum_k c_{m-1,k} \phi_{m-1,k} \right), \phi_{m,l} \right\rangle \\ &= \sum_k c_{m-1,k} \langle \phi_{m-1,k}, \phi_{m,l} \rangle. \end{aligned}$$

Expressing f in terms of the basis functions for W_{m-1} leads to:

$$d_{m,l} = \sum_k c_{m-1,k} \langle \phi_{m-1,k}, \psi_{m,l} \rangle.$$

The inner products are independent of the current decomposition level for the discrete wavelet transform. Therefore,

$$\langle \phi_{m,l}, \phi_{m-1,k} \rangle = h(k-2l), \quad (2.8)$$

$$\langle \psi_{m,l}, \phi_{m-1,k} \rangle = g(k-2l). \quad (2.9)$$

The coefficients of the projection of f into V_m and W_m are given by the following:

$$c_{m,l} = \sum_k c_{m-1,k} h(k-2l), \quad (2.10)$$

$$d_{m,l} = \sum_k c_{m-1,k} g(k-2l). \quad (2.11)$$

The coefficients $c_{m-1,n}$ of f are the starting point of our decomposition, and this leads to a filter bank implementation of the discrete wavelet transform [8]. As seen in Equation 2.10 above, the coefficients $c_{m,l}$ are found by convolving the coefficients $c_{m-1,n}$ with h , and decimating the result by 2. The detail coefficients $d_{m,l}$ are found in similar fashion for the filter g . These equations (2.10 and 2.11), along with similar constructions for the synthesis filters, lead to the filterbank implementation of the discrete wavelet transform, shown in Figure 2.1.

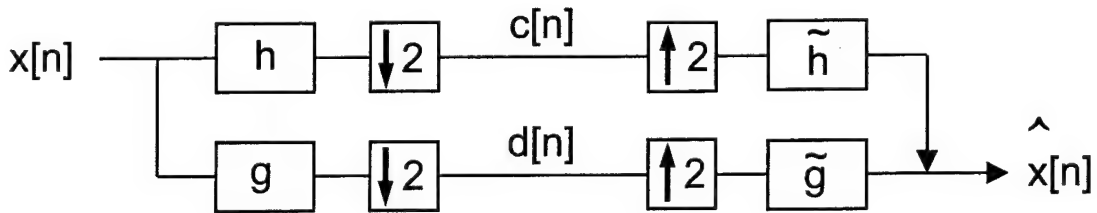


Figure 2.1: Filterbank Implementation of Discrete Wavelet Transform

After determining $c_{m,l}$ and $d_{m,l}$, the function f can be decomposed onto the orthogonal subspaces of V_m , i.e., V_{m+1} and W_{m+1} . The subspaces of V_m can be decomposed using the same formulas because the filters h and g are independent of the decomposition level m and lead to a recursive decomposition. The discrete wavelet transform consists of a set of scaling coefficients $c_m[n]$, which represent coarse signal information at some lowest scale $m = M$, and a set of wavelet coefficients $d_m[n]$, which represent detail signal information at scales $m = 1, 2, \dots, M$.

2.2 Denoising

Denoising is an important concept for image restoration; basically, it is any method used to remove noise from an image. It has been approached in many ways using many different techniques. Denoising methods in the Fourier transform domain and in the wavelet domain will be discussed but only the latter will be employed in this thesis. Although all denoising methods require some a priori information about the statistics of the noise, denoising methods using a priori image information will also be reviewed.

The process of restoring digital images is often approached with some a priori knowledge about the cause of the degradation, typically the statistics of the noise. In many restoration techniques, the degradation is modeled using this knowledge and then the model is used in a way to reverse the effects of the degradation. Many techniques to restore digital images using this kind of information have been studied based on frequency domain concepts [1]. These techniques typically involve some form of lowpass or adaptive filtering in the frequency domain. More direct mathematical approaches have also been studied. Mathematical approaches fit the data in a least mean-

squares sense but also require some degree of smoothness. In the mathematical approaches, the types of a priori knowledge used in image restoration techniques vary between equality and inequality constraints. The constraints contain information on the cause of the degradation in the image. For example, the probability distribution for the noise throughout the image could be known. This image could then be denoised using a form of low-pass filter in the Fourier transform domain or by using thresholding in the wavelet transform domain [2]. The soft-threshold in the wavelet domain provides a smoothness class in the restored image equivalent to or less than the smoothness class held by the original image while maintaining close to a minimum in least squares fitting to the original image. Knowledge about the degradation in an image (in this case, the statistics of the noise) has been effectively used as a priori information to help restore the image [2].

A different approach to image restoration using a priori information involves specific knowledge about the image itself instead of the degradation. Using this technique requires knowledge about the image before the effects of degradation have been introduced. A procedure in the Fourier transform domain using this type of a priori information was developed in [3] and showed some improved performance. That procedure requires full knowledge of one quarter of the image without degradation; this is not always practical. However, the concept in general is valid; information about the image should be a valuable tool for image restoration.

Recently, the wavelet transform has shown great success in reducing the noise in images [2, 4]. A reconstruction method for an unknown function f on $[0,1]$ with additive noise was proposed with excellent results [2]. The method operates on the noisy

measured data $d_i = f(t_i) + z_i$, where $i = 0, \dots, n-1$, $t_i = i/n$, and $z_i \stackrel{iid}{\sim} N(0,1)$. The d_i are transformed into the wavelet domain, and the resulting wavelet coefficients are translated towards zero by the threshold amount $(2*\log(n))^{1/2}*\sigma/(n)^{1/2}$ to form the reconstruction, f_n^* . The reconstruction, f_n^* , proved to be as smooth as f with high probability in many smoothness measures. The estimator of the function obtained from the data fits the unknown function almost as close in the mean square sense as any estimator could fit. These results show how effective soft-thresholding is for noise removal. This is a soft-threshold because coefficients with an absolute value at or below the threshold are set to zero and coefficients with an absolute value greater than the threshold are reduced by the amount of the threshold. Hard-thresholding is also available in wavelet denoising. The hard-threshold is similar to a soft-threshold with the difference being that coefficients with an absolute value greater than the threshold are not modified. However, hard-thresholding typically induces a greater Gibbs phenomenon than soft-thresholding and the reconstruction f_n^* will not be as smooth. Approached from a mathematics standpoint, thresholding yields the best estimate [4].

Even with many image restoration techniques available, research continues in this area due to problems with each of these techniques. Edges in an image provide important object definition but are difficult to deal with in image restoration because they cause discontinuities. Many image restoration techniques do not maintain the very important (visually significant) edges of an image. Low pass filters in the Fourier transform domain remove noise but also cause sharp edges to blur. The Gibbs phenomenon, an interchange of overshooting and undershooting a target level, occurs globally in Fourier-based de-noising. The pseudo-Gibbs phenomenon appears only locally in wavelet-based

de-noising [5]. Whether global or local, the Gibbs phenomenon causes undesirable visual artifacts in the area of discontinuities after de-noising in the Fourier domain or the wavelet domain. Thus, researchers continually attempt to improve image restoration techniques.

2.3 Redundant Wavelets and Denoising

Coifman and Donoho developed a successful technique to weaken the pseudo-Gibbs phenomenon in the wavelet domain [5]. "Cycle spinning" by Coifman "averages out" the translation dependence in the wavelet basis and suppresses the undesired artifacts. In this technique, the wavelet basis functions can be set to shift a limited number of times or set to shift over the full scale of the signal, making the transform "Fully Translation-Invariant." Either of these techniques works well with both hard-thresholding and soft-thresholding in the wavelet domain although typically hard thresholding is used. In most cases, the "Fully Translation-Invariant" system gives the best results in terms of mean-squared error over "cycle spinning" with a limited number of shifts, although both improve performance over non-redundant denoising. A redundant undecimated wavelet transform is also an effective technique for improving image restoration. For images, the wavelet transform is implemented in a separable fashion, i.e., the 1-D wavelet transform is performed on the rows and then the columns. Thus, for images the redundant transform performs the wavelet transform for the image with no shifts, one column shift, one row shift and one of each. This technique repeats at each iteration so the transform becomes very large quickly (growing as a factor of 4^L ,

where L is the number of iterations). Most this information is more than is needed for reconstruction and can therefore be used to improve restoration.

2.4 Other Wavelet-Based Techniques

Other image processing techniques have been developed focusing on the preservation of edges. In an attempt to preserve edges, Belge et. al. used wavelet domain image restoration and adaptive edge-preserving regularization [7]. The distribution of wavelet coefficients for many images is similar to that of a Gaussian density distribution but the tails are much heavier due to edges. This knowledge of the distribution for wavelet coefficients in an image is used to ensure preservation of the important edges in images. The edge-preserving image restoration techniques provide methods to remove noise and degradation while maintaining clear edges, but these methods do have problems in the smooth regions of an image. This technique is an example of an adaptive denoising algorithm.

2.5 Adaptive Wavelet Transforms Via Lifting

The lifting scheme [6] offers a simple implementation to perform the wavelet transform and easily allows for perfect reconstruction back to the spatial domain. The lifting scheme breaks the wavelet transform into a prediction and an update step. Any linear, non-linear, or space-varying function may be used to perform the predict and update. The transform that results is always invertible due to the lifting construction. In the linear prediction step, neighbors of a certain point are used to predict that point. The errors in the prediction create the detail coefficients of the wavelet transform. The

prediction can be performed using one point or several points. These points suppress polynomials up to the order of the number of points used for prediction. The update step uses the detail coefficients in the same manner to update a point and create a coarse coefficient of the wavelet transform. This procedure to perform the wavelet transform is simple, logical and flexible, and will be described in more detail in Chapter 3.

Lifting allows for spatially adaptive and scale adaptive transforms [6]. The adaptive transforms match the characteristics of a signal using the data-based prediction measures of the lifting scheme. For the scale-adaptive transform (ScAT), several points are used for prediction but not all these points are used to suppress the polynomials as in the usual lifting scheme. These extra degrees of freedom are used to adapt to the signal. This adaptation is completed at each scale to minimize the spatially averaged squared prediction error. This adaptive predictor effectively zeros out the dominant signal structure at each scale. The variations from this signal structure are then represented by the detail coefficients of the wavelet transform. The space-adaptive transform (SpAT) changes the wavelet basis function at each point and scale. Lifting allows the predictor to change instantaneously with the signal. In this adaptive algorithm, the predictor is chosen to minimize the detail coefficient of the wavelet transform, which is the error in the prediction. Therefore, the number of points used for prediction in the space-adaptive transform changes from point to point and scale to scale. The adaptive transforms perform almost as well or even superior to the common wavelets for denoising. Again, the available image restoration techniques are improved upon with various algorithms. This thesis will concentrate on the ScAT.

2.6 Summary

Research shows many techniques available for image restoration and image denoising. Certain factors in the Fourier and wavelet domains still cause problems, which are visually undesirable. Various methods improve some of these effects. "Cycle spinning" developed by Coifman provides great improvement over artifacts caused by the pseudo-Gibbs phenomenon in the wavelet domain [5]. The adaptive transforms developed by Claypoole using the lifting technique can improve on wavelet denoising via thresholding [6]. The use of a priori knowledge can also improve the denoising performance. This thesis research will combine wavelets, adaptivity, redundancy, and the use of a priori information. The scale adaptive wavelet transform will be modified to use redundancy, then trained on a known object within an image. This newly adapted transform will then transform the entire degraded image into the wavelet domain where a de-noising threshold will be applied. The inverse transform should yield improvement in the area where the known object is located. A successful algorithm of this type would be desirable in many applications, particularly pattern recognition. When looking for a target in pattern recognition, an algorithm such as this could be run on an image before attempting to locate the target so that the properties of the target would be enhanced, making the target easier to identify by the pattern recognition system. This is just one example of how this type of locally adaptive algorithm could be very useful in image restoration and image processing in general. Variations of the adaptive and redundant wavelet transforms have great potential in enhancing the techniques of image restoration.

III. Methodology

As described in Chapter II, Wavelet transforms compress most signals into a few large coefficients that contain information on both time and frequency. The lifting approach [9, 10, 11] to wavelets will be helpful in this research, providing a structure to easily incorporate adaptivity into the wavelet transform. The lifting interpretation views the wavelet transform as a prediction-error decomposition. The lifting scheme provides easy implementation and a way to introduce adaptivity. Redundancy will also be implemented to reduce the psuedo-Gibbs phenomenon. Adaptive transforms will be utilized so that a set of best predictors can be found for a given image; a priori information containing perfect knowledge of part of the image or an object in the image will be used to train the adaptive transform.

3.1 Lifting

The lifting process is reviewed here. The lifting process is performed in three major steps: the split, predict, and update, which are described below.

Split: The original data is separated into two subsets. Any disjoint split of the data can be made but the usual split in the lifting scheme is the division into even and odd data points. For the one-dimensional data set $x[n]$, the even set would be $x_e[n] = x[2n]$ and the odd $x_o[n] = x[2n+1]$. Clearly, the output of the split is time-varying.

Predict: The error in predicting $x_o[n]$ from $x_e[n]$ creates the wavelet coefficients $d[n]$ using the prediction operator P :

$$d[n] = x_o[n] - P(x_e[n]). \quad (3.1)$$

Update: The update step forms a coarse approximation to the original signal $x[n]$ in the scaling coefficients $c[n]$. They are formed by combining $x_e[n]$ and the update operator U applied to the wavelet coefficients, $d[n]$:

$$c[n] = x_e[n] + U(d[n]). \quad (3.2)$$

Multiple iterations of the lifting process are accomplished by repeating these steps on the scaling coefficients, $c[n]$ to create a complete set of scaling and wavelet coefficients. At each iteration, the scaling and wavelet coefficients can be weighted to normalize the energy of the underlying wavelet functions.

Inversion of the lifting steps is easily accomplished, regardless of the condition of P and U , by rearranging Equations (3.1) and (3.2). The forward and inverse lifting transforms use the same P and U to perfectly reconstruct the transformed signal. The forward and inverse lifting stages are shown in Figures (3.1) and (3.2) respectively. Note that these figures depict the optional 4th step, the weighting of the wavelet and scaling coefficients with k_e and k_o , respectively.

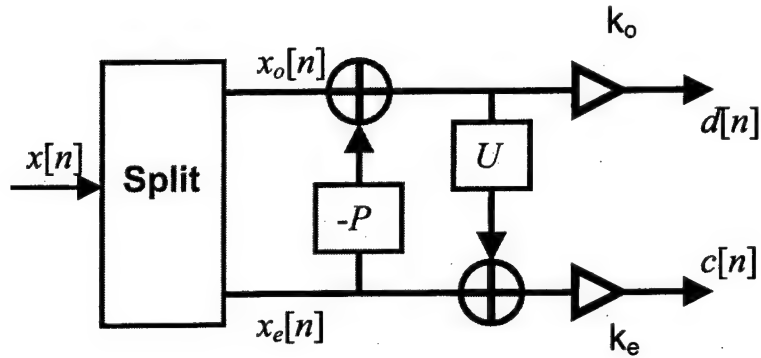


Figure 3.1: Forward Lifting Stage.

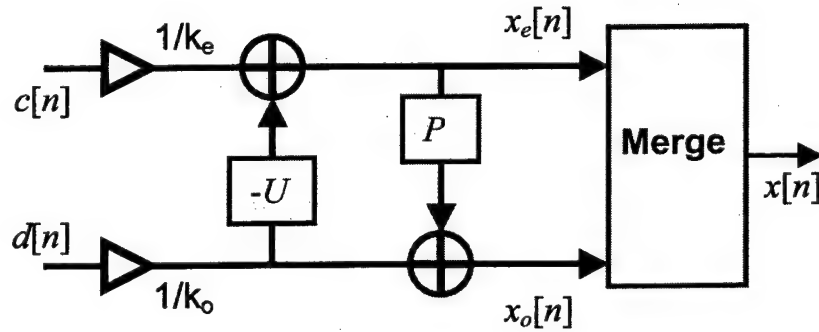


Figure 3.2: Inverse Lifting Stage.

In the standard (linear) lifting scheme, an N -point predictor design is found using the desired predictor's z -transform. For a 4-point predictor, the z -transform is $P(z) = p_1 z^{-1} + p_2 + p_3 z + p_4 z^2$. An illustration to create the wavelet coefficient $d[n]$ from

$x_e[n]$, $x_o[n]$, and P is shown in Figure 3.3. By tracking the effect of P up through the tree, an equivalent prediction vector g can be determined. The prediction vector g would be applied to the original data, $x[n]$. In this case, $g = [-p_1, 0, -p_2, 1, -p_3, 0, -p_4]^T$. Placing zeros in the locations corresponding to odd data points except for the center one accounts for the split step and allows the vector g to be applied to the original data.

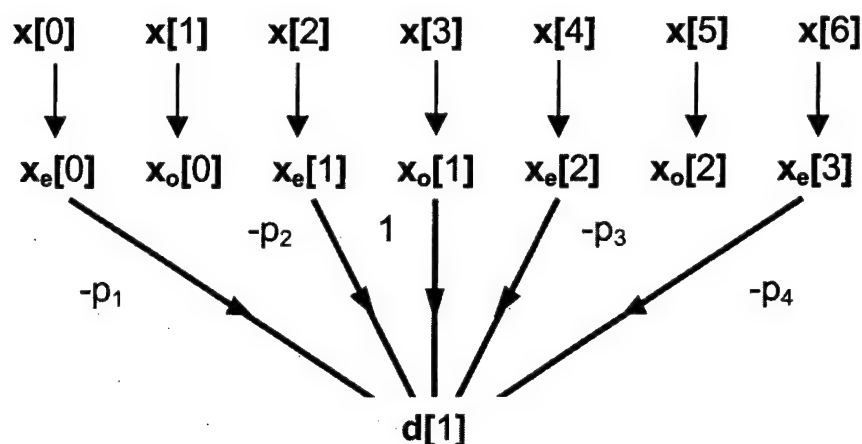


Figure 3.3: Prediction Design.

Now for the N -point predictor, an $N \times 2N-1$ Vandermonde matrix V is formed. The entries of the Vandermonde matrix $[V]_{k,n} = (n-l)^k$, where $n = 1, 2, \dots, 2N-1$ and $k = 0, 1, \dots, N-1$ and $l=N$ if a balanced filter is desired. Otherwise l is the number from 1 to $2N-1$ that causes the column, where $n-l = 0$, to correspond to the 1 in g . All even columns are deleted to create a new matrix V^\diamond . Vg must equal zero so that all low-order polynomials are suppressed by the predictor and thus $V^\diamond p = [1 \ 0 \dots 0]^T$. Now, p can easily be found by solving this set of linear equations.

The update filter uses an even data point and \tilde{N} of the wavelet coefficients to create a coarse coefficient. It is not necessary for \tilde{N} to equal the number of prediction coefficients, N . The prediction coefficients are necessary to find the update filter in the normal lifting scheme. Again, the z-transform, $U(z) = u_1 z^{-2} + u_2 z^{-1} + u_3 + u_4 z$, is used to find the update filter. The update coefficients u_k and the prediction coefficients p_k combine to form the update filter \mathbf{h} which should pass low-order polynomials on to the coarse coefficients $c[n]$ and attenuate high-order polynomials. A 4-point update follows a 2-point prediction in Figure 3.4 and tracing the effects of P and U to the original data gives the following update vector \mathbf{h} :

$$\mathbf{h} = [-p_1 u_1, u_1, -p_1 u_2 - p_2 u_1, u_2, 1 - p_2 u_2 - p_1 u_3, u_3, -p_2 u_3 - p_1 u_4, u_4, -p_2 u_4]^T.$$

The mirror update filter vector $\tilde{\mathbf{g}}$ where $\tilde{\mathbf{g}}_n = (-1)^n \mathbf{h}_n$ is created to suppress low-order polynomials.

$$\tilde{\mathbf{g}} = [-p_1 u_1, -u_1, -p_1 u_2 - p_2 u_1, -u_2, 1 - p_2 u_2 - p_1 u_3, -u_3, -p_2 u_3 - p_1 u_4, -u_4, -p_2 u_4]^T.$$

With the previously determined prediction coefficients p_k , only the update coefficients u_k are left to be determined. The update coefficients are found by solving $\mathbf{V}\tilde{\mathbf{g}} = 0$, i.e., just as in the design of the predictor, the mirror filter $\tilde{\mathbf{g}}$ is design to suppress low order polynomials. Thus, the filter \mathbf{h} will preserve these low order polynomials, yielding the desired coarse approximation.

PCUSER1

Microsoft Word – Master Thesis.doc
03/09/01 04:18 PM



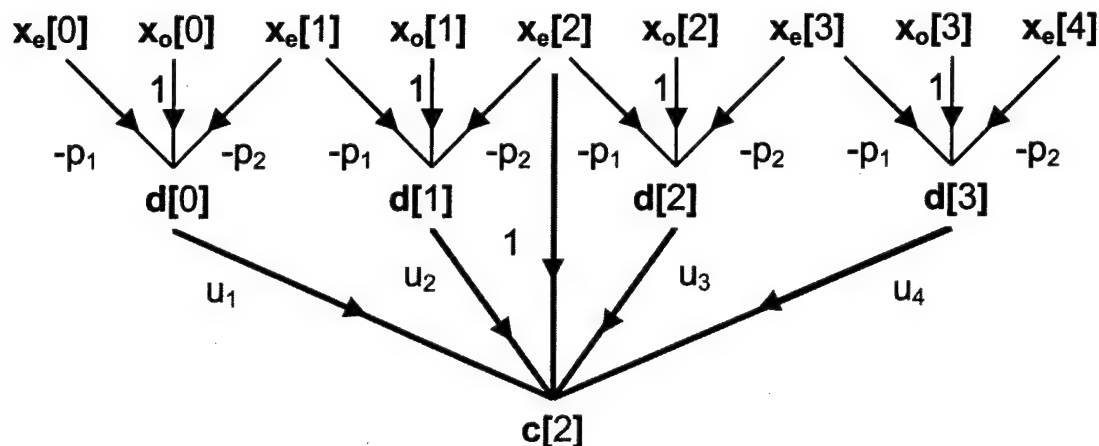


Figure 3.4: Update Design.

With the lifting procedure, the transition to the wavelet domain is made through the steps of split, predict, and update. The prediction step is designed to eliminate low-order polynomial signal structures. The wavelet coefficients formed by the prediction step maintain the high-order polynomials as the details. Then, the update is designed so that the low-order polynomial signal structure is preserved at the next coarser scale.

3.2 Wavelet Polyphase Representation

The lifting wavelet transform can be written in the form of a perfect reconstruction multirate filter bank. A perfect reconstruction multirate filter bank can be created using any biorthogonal wavelet transform.

Separating each wavelet filter into the polyphase components where $H(z) = H_e(z^2) + z^{-1}H_o(z^2)$, the discrete wavelet transform can be completed as in Figure 3.5.

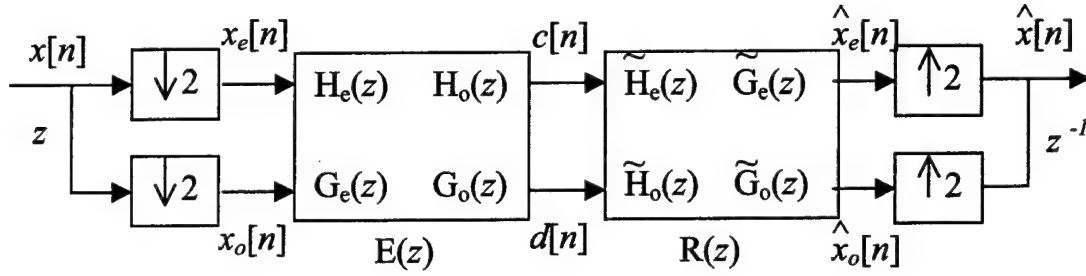


Figure 3.5: Polyphase Form of Wavelet Transform.

In this form, down sampling the signal by two and then applying the filter $H_e(z)$ is the same as filtering using $H_e(z^2)$ and then down sampling by two [13].

For the lifting scheme when the odd/even split is made, the polyphase domain is created. In Figure 3.6, the polyphase matrices are created using the predict and update steps.

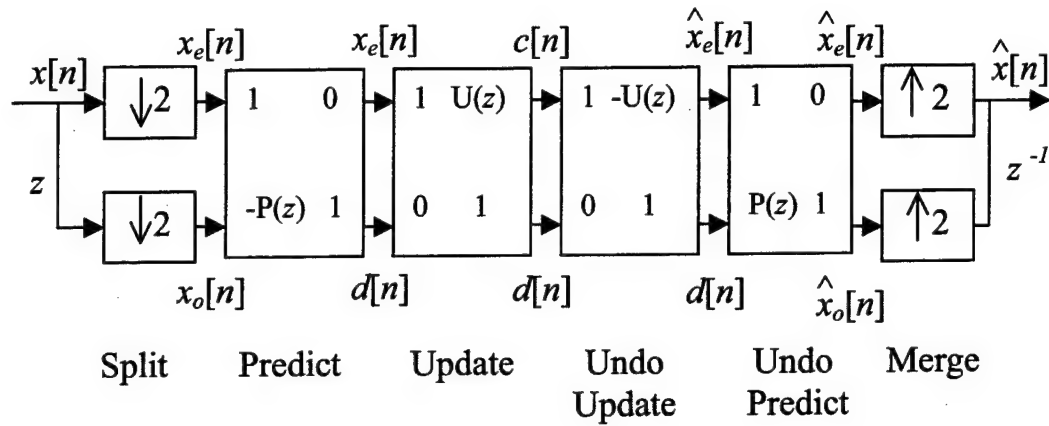


Figure 3.6: Lifting operations in Polyphase Form.

The wavelet coefficients $d[n]$ and the scaling coefficients $c[n]$ are created just as before in Equations (3.1) and (3.2). The prediction matrix does not change the even data points $x_e[n]$ and the update matrix does not change the wavelet coefficients $d[n]$. The prediction matrix forms the wavelet coefficients $d[n]$ as the difference in the odd data $x_o[n]$ and $P(x_e[n])$. The update matrix forms the scaling coefficients $c[n]$ as the sum of even data $x_e[n]$ and $U(d[n])$, the update applied to the wavelet coefficients.

Combination of the predict and update steps and the undo update and undo predict steps leads to the lifting scheme in polyphase form with matrices $E(z)$ and $R(z)$ in Figure 3.7.

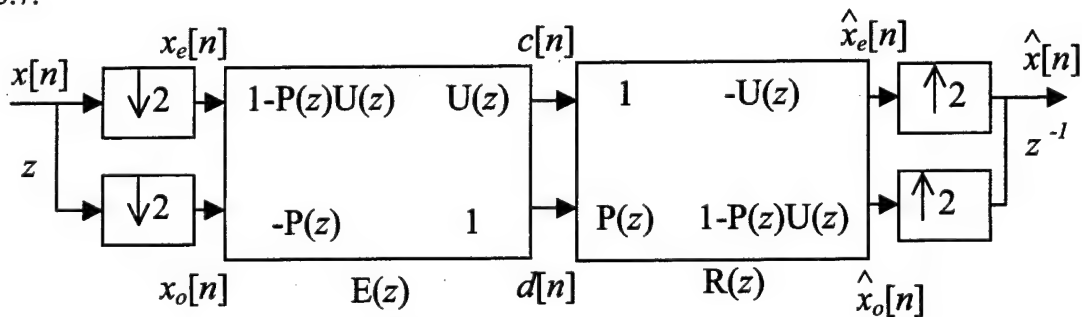


Figure 3.7: Combination of Lifting Steps in Polyphase Form.

The lifting scheme typically does not lead to orthogonal transforms. This would only be possible if $P(z)$ and $U(z)$ were constants. Therefore, the lifting transform is generally viewed as a biorthogonal wavelet transform. From the combination of steps in Figure 3.7, the wavelet filters in terms of the lifting scheme are as follows:

$$\begin{aligned} H_e(z) &= 1 - P(z)U(z) \\ H_o(z) &= U(z) \\ G_e(z) &= -P(z) \\ G_o(z) &= 1 \end{aligned}$$

and therefore,

$$\begin{aligned} H(z) &= 1 - P(z^2)U(z^2) + z^{-1}U(z^2) \\ G(z) &= -P(z^2) + z^{-1}. \end{aligned} \tag{3.3}$$

The wavelet filters $h[n]$ and $g[n]$ are related to the scaling (ϕ) and wavelet (ψ) functions by the following wavelet recursion relations [8]

$$\begin{aligned} \phi(t) &= \sum_k h[k]\phi(2t-k) \\ \psi(t) &= \sum_k g[k]\phi(2t-k). \end{aligned} \tag{3.4}$$

Using the wavelet filters created from the lifting scheme, vanishing moment constraints on $\psi(t)$ can be mapped into constraints on the prediction and update filters P . Adding a zeroth vanishing moment to $\psi(t)$,

$$\int_{-\infty}^{\infty} \psi(t)dt = \int_{-\infty}^{\infty} \sum_k g[k]\phi(2t-k)dt = 0$$

and switching the order, then $\int \phi(2t-k)dt$ is equal to a constant m_0 , not zero. Leaving $m_0 \sum_k g[k]=0$ and since $G(z)=-P(z^2)+z^{-1}$, the zeroth vanishing moment constraint makes

$$p_1 + p_2 \dots + p_N = 1.$$

Forcing the prediction filter to eliminate zeroth order polynomials leads to the same constraint. Additional vanishing moments in the analysis wavelet function is equivalent to eliminating additional polynomials in the prediction step. After determining the coefficients for the prediction filter or $G(z)$, vanishing moments are added to the synthesis wavelet function $\tilde{\psi}(t)$ with the following

$$\int_{-\infty}^{\infty} t^l \tilde{\psi}(t) dt = \int_{-\infty}^{\infty} \sum_k \tilde{g}[k] t^l \phi(2t-k) dt = 0.$$

This equations utilizes the equivalent recursion relation for the dual (synthesis) filters, as in Equation 3.4 above. Thus, each vanishing moment on the synthesis wavelet function $\tilde{\psi}(t)$ is equivalent to an additional update filter polynomial constraint. The biorthogonal wavelet system created by adding vanishing moments to the underlying wavelet functions is the same as eliminating and preserving polynomials in the predict and update steps. Constraints on the wavelet filters h, g, \tilde{h} , and \tilde{g} are identical whichever approach is used to create them. The lifting scheme does not require the use of the polyphase matrices or the underlying scaling and wavelet functions making its implementation easier. This also allows for nonlinearities and adaptivity to be introduced into the wavelet transform. The properties of the underlying wavelet transform can be controlled by forcing the prediction and update filters to meet requirements besides low-order polynomial suppression. In other words, the transform can adapt by forcing the

predict and update filters to suppress the training signal, while still maintaining some vanishing moments properties of the standard wavelet transform.

3.3 Redundancy

Superior performance in many applications is gained by using a redundant wavelet transform [5]. When denoising, the pseudo-Gibbs phenomenon appears in the local area of discontinuities after thresholding the non-redundant wavelet transform coefficients. The shift invariant or redundant transform improves thresholding by averaging over all possible shifts of the signal. The redundant lifting scheme is shown in Figure 3.8 for a one-dimensional signal.

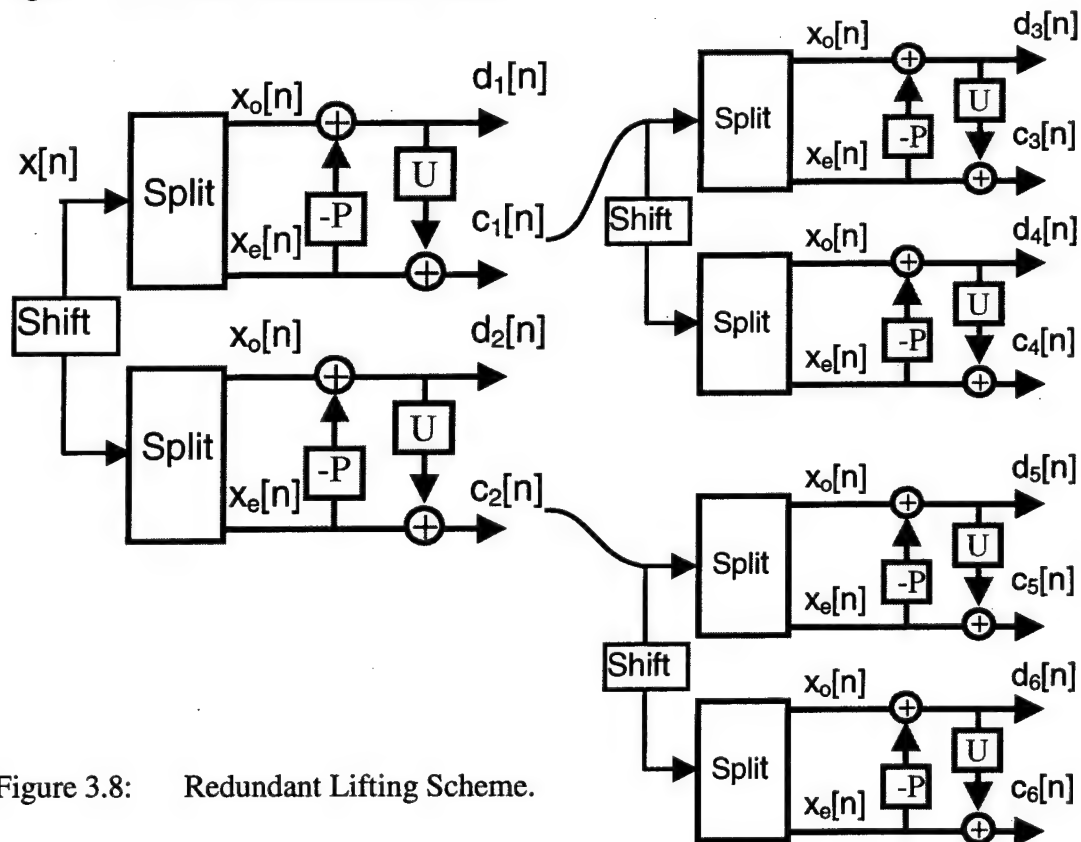


Figure 3.8: Redundant Lifting Scheme.

This method of shifting over all possible shifts and transforming is known as “cycle spinning” and was developed by Coifman to “average out” translation dependence [5]. Implementation of the redundant lifted transform on images will create two additional shifts for one iteration, i.e., four transforms for one image. As iterations L increase the size of the data increases by 4^L . This causes a problem in storing and displaying the transform. Instead of storing each possible shift as a complete transform (which would create four transforms the same size as the original image) the transforms will be stored as a four dimensional array. The first two dimensions are the size of the original image, the third is always four for the first four transforms created at the first iteration, and the fourth dimension is equal to the number of iterations. Thus, a transform of a 256×256 image with 3 iterations would have a redundant wavelet transform dimension of (256, 256, 4, 3) and 4 iterations of the same image would have a dimension of (256, 256, 4, 4). For ease of storage and display purposes, this method will retain all coarse approximations at each scale, even though only the lowest level coarse approximation is needed for reconstruction.

3.4 Adaptivity

The lifting scheme was demonstrated in Section 3.1 using polynomial constraints but restrictions besides low-order polynomial suppression can be implemented. This research uses the scale-adaptive transform to adapt the predictor of each lifting stage to match a training signal structure at that scale. A N -point predictor is used to suppress polynomials up to order M , less than N . This is equivalent to adding M vanishing moments to the underlying wavelet function. The other degrees of freedom will adapt to

the training signal. The remaining $N-M$ degrees of freedom optimize the predictor so that it minimizes the spatially-averaged squared prediction error. Therefore, the predictor matches both polynomial and non-polynomial signal structure at each scale. A N -dimensional constrained least-squares problem solves this optimization using the constraint that the predictor must suppress $M < N^{\text{th}}$ order polynomials. The goal is to minimize the sum of squared prediction errors, $\mathbf{e}^T \mathbf{e}$, when $\mathbf{e} = \mathbf{x}_o - \mathbf{X}_e \mathbf{p}$. Here, \mathbf{x}_o are the odd data points, \mathbf{X}_e is a matrix of the even points such that $[\mathbf{X}_e]_{n,k} = x_e[n-k]$ and \mathbf{p} is the vector of prediction filter coefficients. \mathbf{X}_e and \mathbf{p} are attempting to predict \mathbf{x}_o . Solving $\min_{\mathbf{p}} \|\mathbf{x}_o - \mathbf{X}_e \mathbf{p}\|^2$ subject to $\mathbf{V}^o \mathbf{p} = [1, 0 \dots 0]^T$ results in a \mathbf{p} that minimizes $\mathbf{e}^T \mathbf{e}$, and maintains M polynomial constraints. In this case, \mathbf{V}^o is an $M \times N$ matrix containing the first M rows of the full rank Vandermonde matrix \mathbf{V}^\diamond as determined in Section 3.1. The predictor now tries to capture the dominant training signal structure at each scale. When this transform is applied to the degraded image, the noisy signal variation from the training signal structure is represented by the wavelet coefficients $d[n]$. The update filter is designed so that the coarse signal approximation transformed at the next scale should maintain the low frequency dominant structure of the training signal.

3.5 Denoising/Thresholding

An adaptive transform is being implemented and thus, an appropriate adaptive threshold will be created for denoising so that each sub-band in each iteration will have its own adaptive threshold. The a priori information used to train the signal will also help determine the threshold for noise removal. While implementing this redundant transform, the transform must be completed on the training image as well as the noisy

image for each shift and iteration. This information gives us not only the training data for the next scale but it also gives a comparison for the size of the wavelet coefficients $d[n]$. Looking separately at each band a threshold is set as the mean absolute value of the differences in the wavelet coefficients for each of the four bands LL, HL, LH, and HH. Thresholds are set for the LL bands but these bands are not thresholded. The difference in the wavelet coefficients for the training image and the noisy image represent the noise and is a good indicator to help establish an appropriate threshold.

IV. Results

In this chapter, the success of denoising with the redundant adaptive wavelet transform using a priori information is demonstrated. As discussed in Chapter 2, current image restoration techniques have certain undesirable effects. In this research, a new technique, combining adaptive wavelets, redundancy, and a priori information was developed. This thesis research gives reasons why such an algorithm should be powerful to image-processing techniques. Now, the performance of this algorithm is compared to other redundant wavelet-based techniques.

4.1 Error Measures

Two errors measures are used to measure the performance of the adaptive algorithm. The peak signal-to-noise ratio (PSNR) is used to help determine the strength of the true signal compared to the reconstructed signal (or noisy signal).

$$\text{PSNR} = 20 * \log_{10} \left(\frac{\max |x_i|}{\sqrt{\frac{\sum (x_i - \hat{x}_i)^2}{N}}} \right) \quad (4.1)$$

where x_i is the i^{th} pixel of the original image, \hat{x}_i is the i^{th} pixel of the reconstructed (or noisy) image, and N is the total number of pixels. The PSNR values are determined before noise removal and after for comparison of the improvement made in the reconstructed image. PSNR is a common metric in the image processing community.

The second measure of performance used for the algorithm is L^∞ . The error here is the maximum difference in the desired image and the denoised image. This metric relates to the human visual system, and is a good indicator of the visual “quality” of an image. These performance measures are good indicators of how the training algorithm compares to other types of wavelet denoising.

4.2 Denoising Experiments

Several wavelet transforms are used to transform an image. The image is then denoised while in the wavelet domain before it is reconstructed. For a basis comparison, a (4,4) lifting scheme is used with 4 vanishing moments so that the transform is not adaptive and does not take advantage of any a priori information. Also for comparison, a separate baseline case is completed. In this case, the (4,4) lifting transform is used with only 2 vanishing moments and this transform adapts to the noisy image. In other words, this transform is not trained using the a priori information but it does use adaptivity. For each of these transforms, a soft threshold was used with the threshold being 3 times the standard deviation of the noise. A hard threshold was also completed on these transforms using 3.6 times the standard deviation of the noise as the threshold. These are the standard thresholds experimentally derived from [12].

One test of the training algorithm is completed using a (4,4) lift with 2 vanishing moments adapted to the training image and for consistency to the baseline comparisons, a soft threshold equal to 3 times the standard deviation of the noise and a hard threshold equal to 3.6 times the standard deviation of the noise. A second test of the algorithm also uses a (4,4) lift with 2 vanishing moments adapted to the training image and for denoising

uses the threshold set adaptively by the training algorithm as discussed in Chapter 3. This threshold was multiplied by various constants to find which produced the best results and then used for denoising. With a soft threshold, the adaptive threshold is multiplied by a constant of 1.5 for the best results. When a hard threshold is used, the adaptive threshold is multiplied by a constant of 3 for the best results. So one test uses the a priori information to train the transform but uses a standard threshold and the second test uses the a priori information to train the transform and to set the adaptive threshold.

The original image is made zero mean and is show in Figure 4.1. To obtain the training image in Figure 4.2, a part of the original image is made zero mean and then padded with zeros so that it is the same size as the test image. This is necessary because the algorithm calls for an equal number of iterations of the wavelet transform to be completed on both the original image and the training image and therefore to make this possible at all times, the images must be the same size.

4.3 Denoising Results

The first noisy image in Figure 4.3 is created by adding a noise amount of approximately 25 times the standard deviation of the noise giving a PSNR value of approximately 20 dB and a L^∞ measurement of 105.38. This represents a high amount of noise for the image.

Results after using a soft threshold are looked at first. The image reconstructed after using a non-adaptive transform and a standard threshold has significant blurring around the edges of the image, but the PSNR is improved by approximately 8 dB. This

first baseline case is shown in Figure 4.4. The second baseline, in Figure 4.5, case improves the PSNR and the L^∞ measures for the whole image but blurring is still present.

Again looking at the soft threshold results, the test using an adaptive threshold and the training algorithm reduces blurring but effects of the noise are still present, see Figure 4.6. The PSNR values are comparable to the baseline measurements and the L^∞ values are reduced. Using the training algorithm with the standard threshold (Figure 4.7) produces an image that is visually as good as the first baseline case, possibly even a little less blur. The error values are not significantly reduced but are comparable. All soft threshold results with this high noise case cause some blurring of the edges.

Most hard thresholds improve over their equivalent soft thresholds. The hard threshold results are visibly better because there is less blurring. In Figure 4.8, the first baseline case is an improvement over previous transforms but the edges still acquire undesired effects. In Figure 4.9, adapting to the noisy signal leaves obvious artifacts in the reconstructed image but edge effects are not as obvious. Artifacts left from the noise are not as prominent in Figure 4.10. This reconstructed image has less blur, yet it is also smoother. The best PSNR value for the high noise case is produced by Figure 4.11 where the training algorithm is used with the standard threshold. This test also gives a good L^∞ value.

The training error measurements were very similar to the overall picture measurements. This was probably because the majority of the edges in the image were within the training area without any large smooth areas as those found outside of this training area.

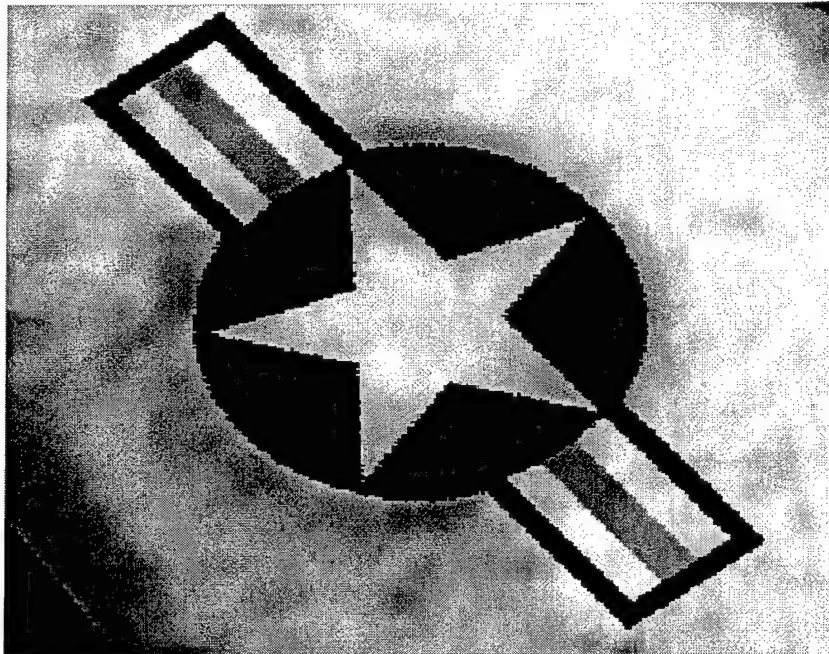


Figure 4.1: Original star image before the addition of noise.

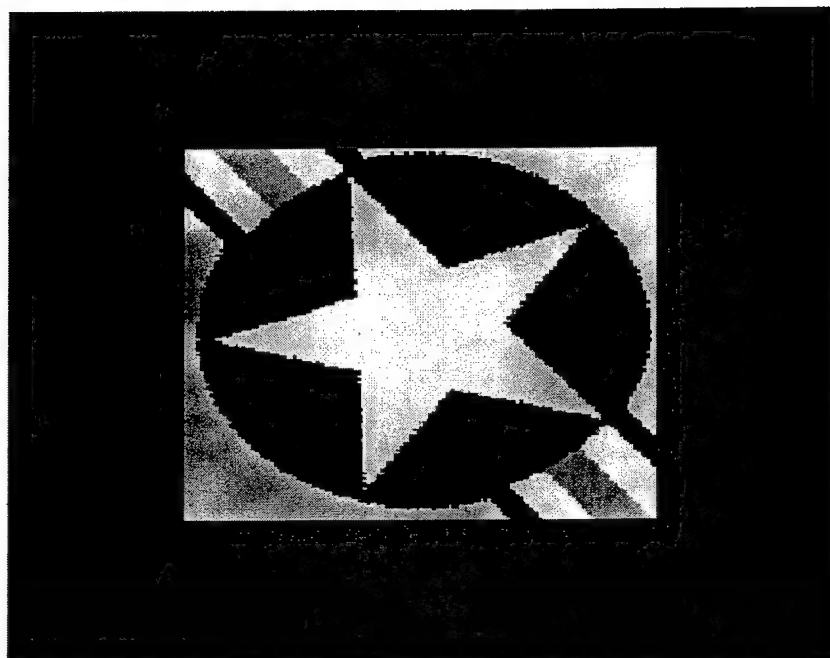


Figure 4.2: Training star image used for adapting the transform.

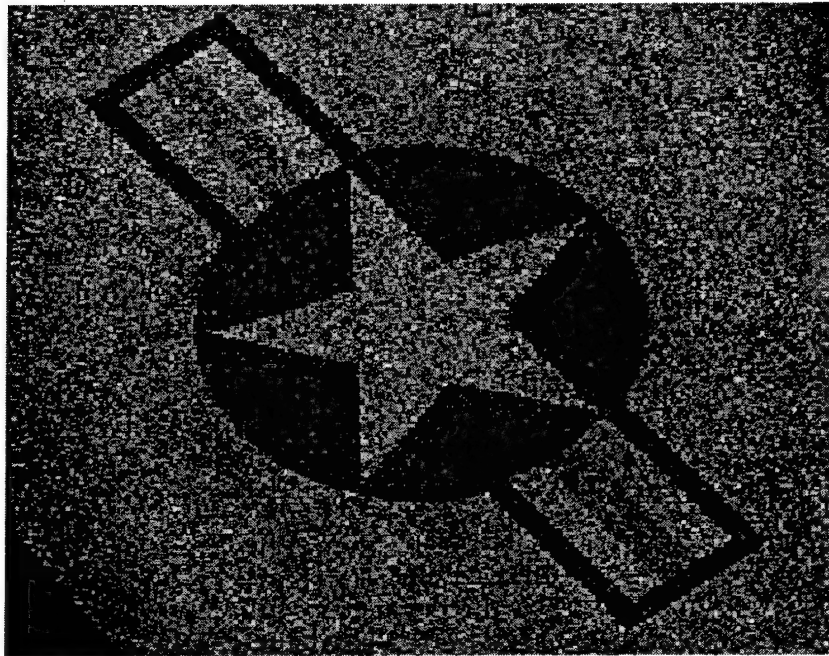


Figure 4.3: Star image and additive Gaussian noise with standard deviation equal to 10% of the maximum signal value (high noise case). For entire image, PSNR = 20.15 dB and $L^\infty = 105.38$. In the training area, PSNR = 20.12 dB and $L^\infty = 105.38$.

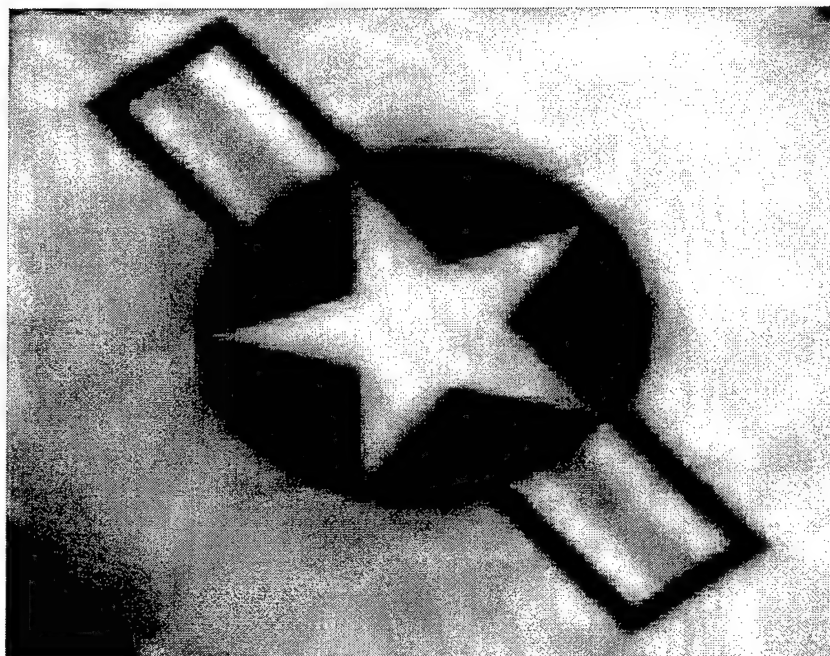


Figure 4.4: Star image denoised using (4,4) lift, 4 vanishing moments (non-adaptive) and a soft threshold equal to 3 times the standard deviation of the noise. For entire image, PSNR = 28.00 dB and $L^\infty = 84.96$. In the training area, PSNR = 25.86 dB and $L^\infty = 66.14$.

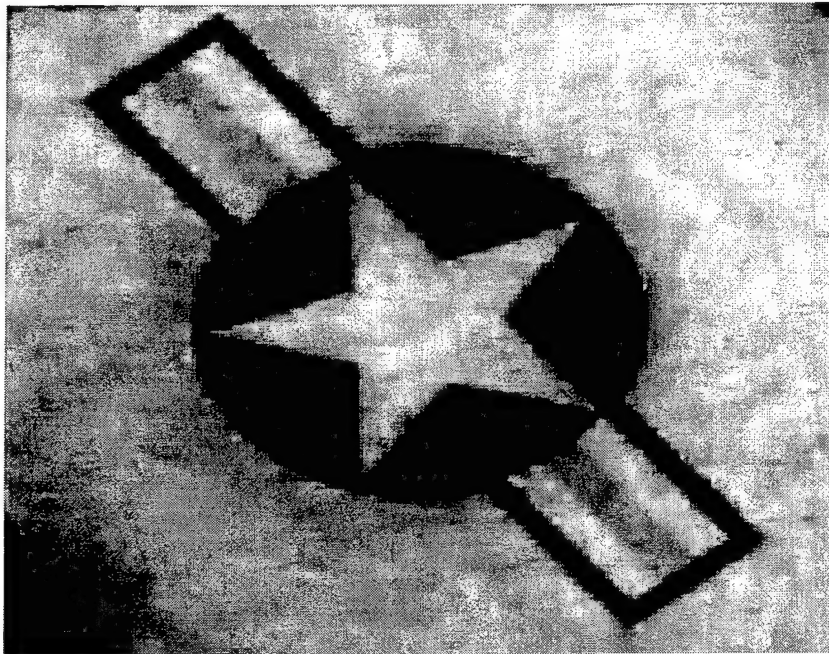


Figure 4.5: Star image denoised using (4,4) lift, 2 vanishing moments, adaptive to noisy signal and a soft threshold equal to 3 times the standard deviation of the noise. For entire image, PSNR = 29.09 dB and $L^\infty = 80.16$. In the training area, PSNR = 27.15 dB and $L^\infty = 67.20$.

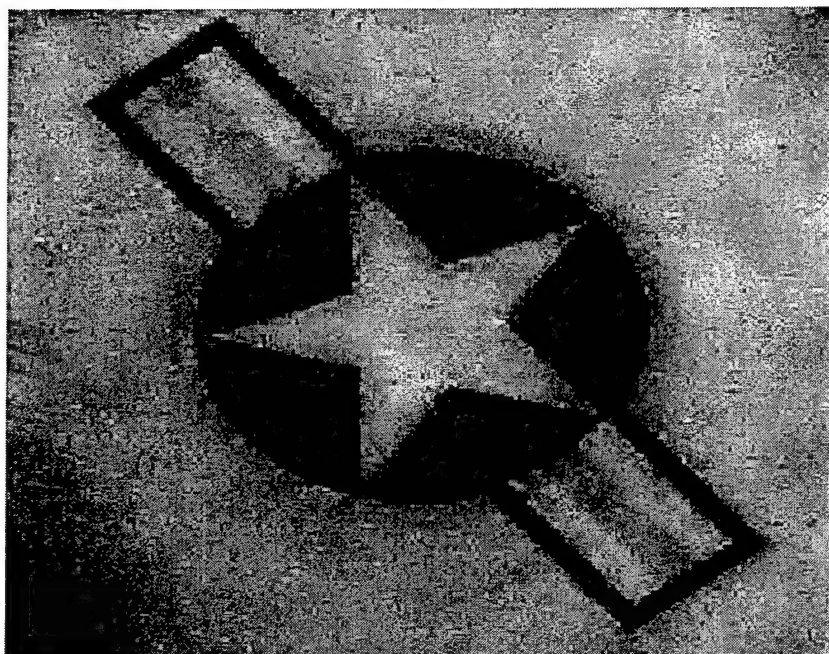


Figure 4.6: Star image denoised using (4,4) lift, 2 vanishing moments, adaptive to training signal and a soft threshold equal to 1.5 times the adaptive threshold set by the transform. For entire image, PSNR = 27.44 dB and $L^\infty = 76.67$. In the training area, PSNR = 26.03 dB and $L^\infty = 66.02$.

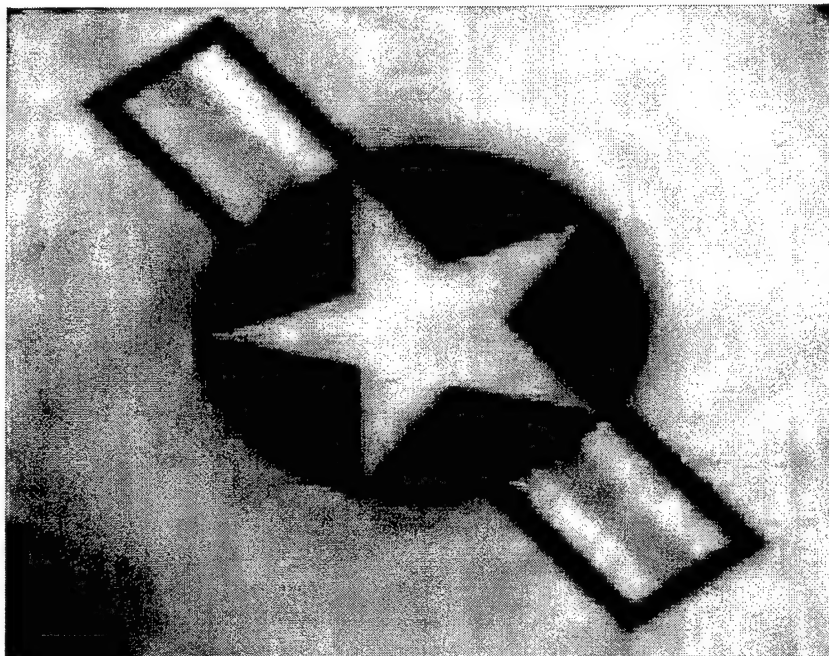


Figure 4.7: Star image denoised using (4,4) lift, 2 vanishing moments, adaptive to training signal and a soft threshold equal to 3 times the standard deviation of the noise. For entire image, $\text{PSNR} = 28.43 \text{ dB}$ and $L^\infty = 86.09$. In the training area, $\text{PSNR} = 26.33 \text{ dB}$ and $L^\infty = 68.66$.

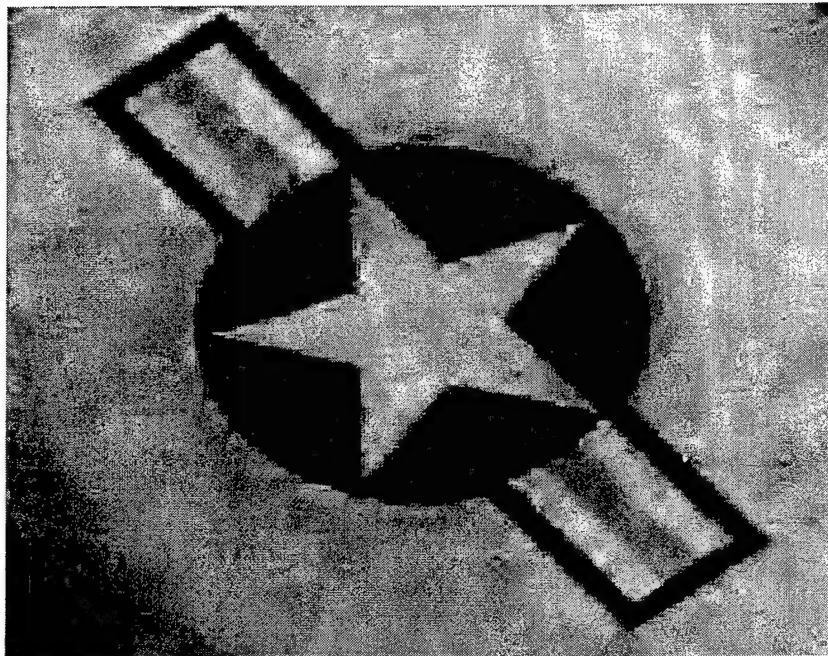


Figure 4.8: Star image denoised using (4,4) lift, 4 vanishing moments (non-adaptive) and a hard threshold equal to 3.6 times the standard deviation of the noise. For entire image, PSNR = 29.91 dB and $L^\infty = 71.68$. In the training area, PSNR = 27.73 dB and $L^\infty = 64.80$.

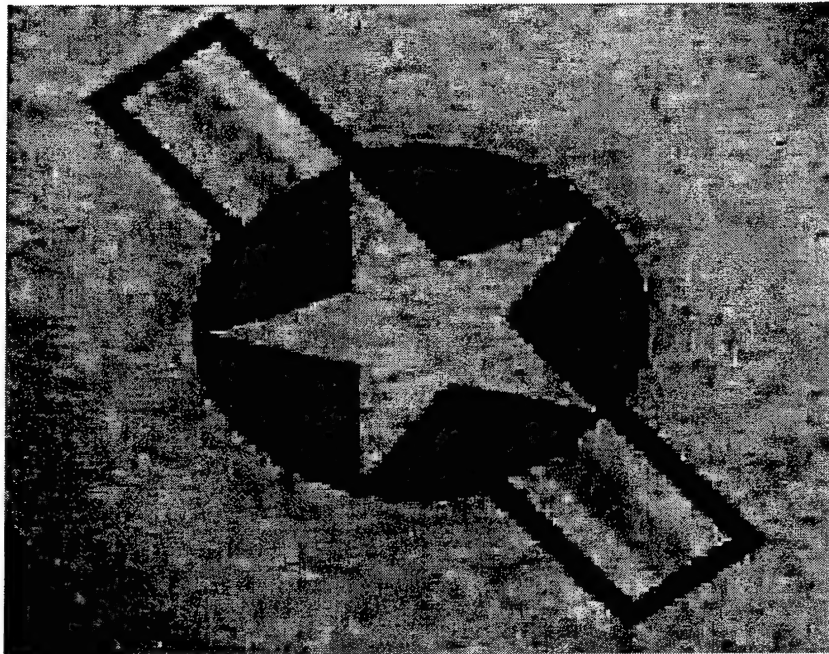


Figure 4.9: Star image denoised using (4,4) lift, 2 vanishing moments, adaptive to noisy signal and a hard threshold equal to 3.6 times the standard deviation of the noise. For entire image, $\text{PSNR} = 28.82 \text{ dB}$ and $L^\infty = 75.20$. In the training area, $\text{PSNR} = 27.39 \text{ dB}$ and $L^\infty = 75.20$.

The second noisy image in Figure 4.12 is created by adding a noise amount of approximately 15 times the standard deviation of the noise giving a PSNR value of approximately 25 dB and a L^∞ measurement of 105.38. This represents a medium amount of noise for the image.

Soft threshold results are looked at first. The image reconstructed after using a non-adaptive transform and a standard threshold has blurring around the edges of the image, but the PSNR is improved by approximately 5 dB. This first baseline case is shown in Figure 4.13. The second baseline, in Figure 4.14, case improves the PSNR and the L^∞ measures for the whole image but blurring is still present.

Again looking at the soft threshold results, the test using an adaptive threshold and the training algorithm reduces blurring but effects of the noise are still present, see Figure 4.15. The PSNR values are comparable to the baseline measurements and the L^∞ values are significantly reduced. Using the training algorithm with the standard threshold (Figure 4.16) produces an image that is visually as good as the first baseline case, and has some improvements in the measurements.

Most hard thresholds improve over their equivalent soft thresholds. The hard threshold results are visibly better because there is less blurring. In Figure 4.17, the first baseline case is an improvement over previous transforms but the edges still blur. In Figure 4.18, adapting to the noisy signal leaves obvious artifacts in the reconstructed image but edges are clearer. Artifacts left from the noise still exist but are reduced in size for Figure 4.19. This adaptive hard threshold used with the training algorithm gives excellent L^∞ values in this example. Figure 4.20 produces the best PSNR value for the

medium noise case which is where the training algorithm is used with the standard threshold. This test also gives a good L^∞ value.

The training error measurements were very similar to the overall picture measurements. This was probably because the majority of the edges in the image were within the training area without any large smooth areas as those found outside of this training area.

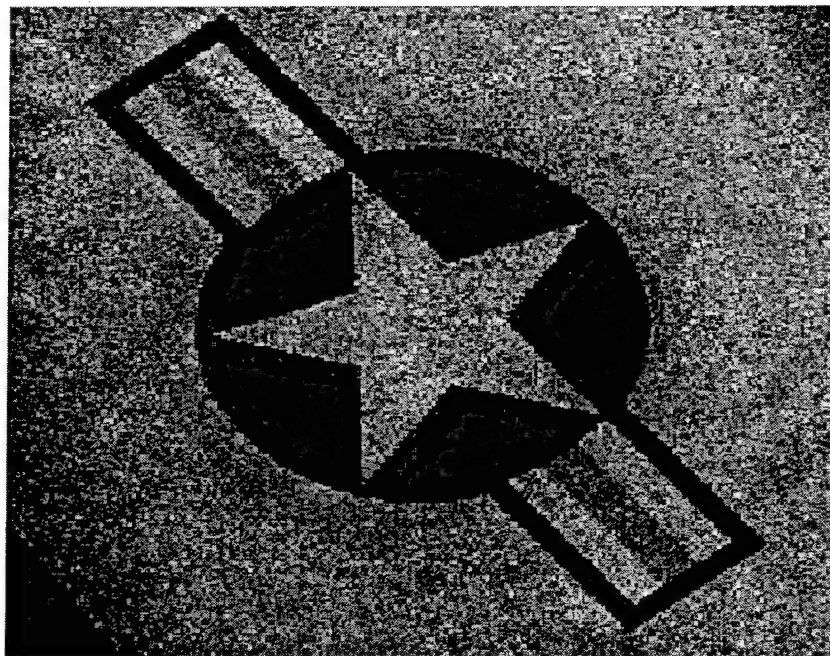


Figure 4.12: Star image and additive Gaussian noise with standard deviation equal to 6% of the maximum signal value (medium noise case). For entire image, PSNR = 24.58 dB and $L^\infty = 63.23$. In the training area, PSNR = 24.56 dB and $L^\infty = 63.23$.

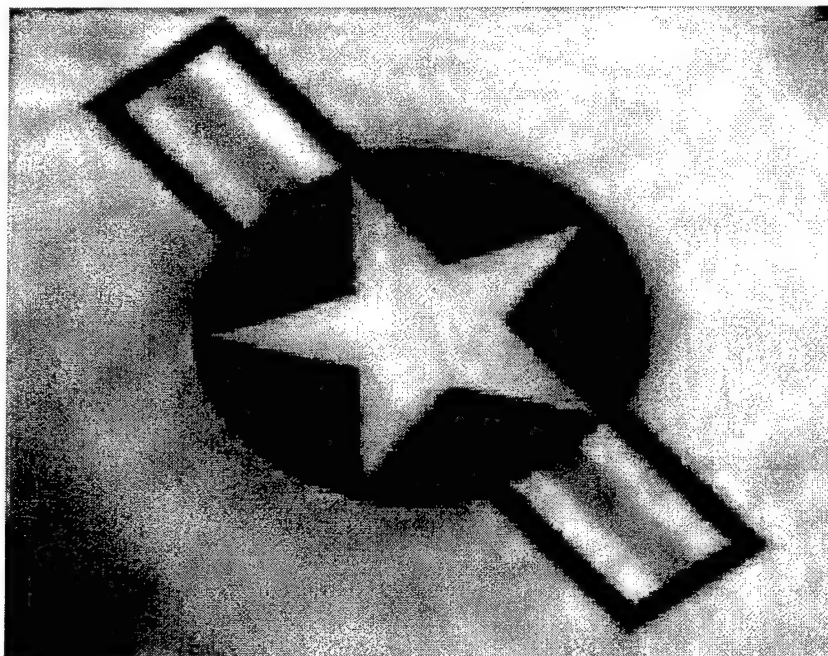


Figure 4.13: Star image denoised using (4,4) lift, 4 vanishing moments (non-adaptive) and a soft threshold equal to 3 times the standard deviation of the noise. For entire image, PSNR = 29.88 dB and $L^\infty = 70.87$. In the training area, PSNR = 27.69 dB and $L^\infty = 58.83$. (medium noise)

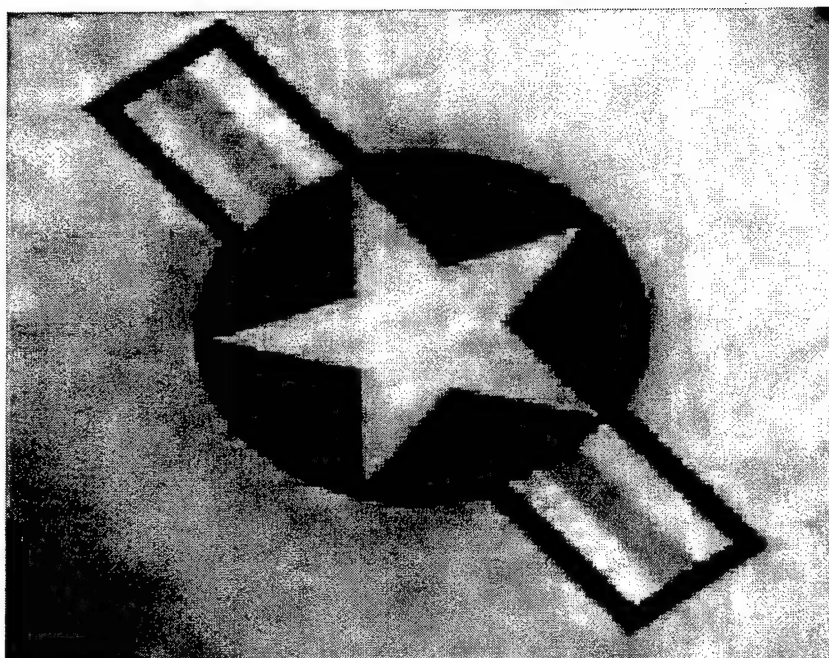


Figure 4.14: Star image denoised using (4,4) lift, 2 vanishing moments, adaptive to noisy signal and a soft threshold equal to 3 times the standard deviation of the noise. For entire image, $\text{PSNR} = 30.91 \text{ dB}$ and $L^\infty = 66.62$. In the training area, $\text{PSNR} = 28.81 \text{ dB}$ and $L^\infty = 55.76$.

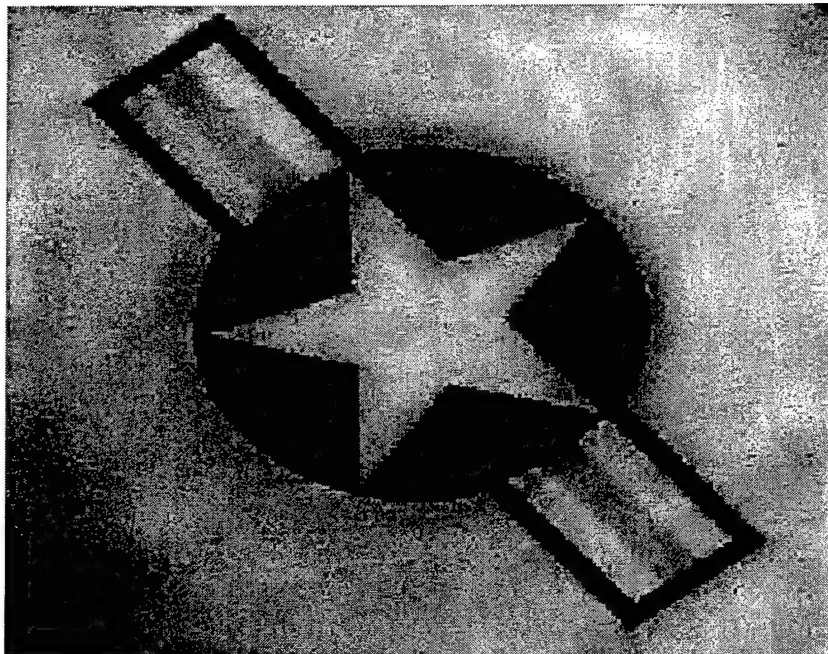


Figure 4.15: Star image denoised using (4,4) lift, 2 vanishing moments, adaptive to training signal and a soft threshold equal to 1.5 times the adaptive threshold set by the transform. For entire image, PSNR = 29.92 dB and $L^\infty = 57.74$. In the training area, PSNR = 28.34 dB and $L^\infty = 50.86$.

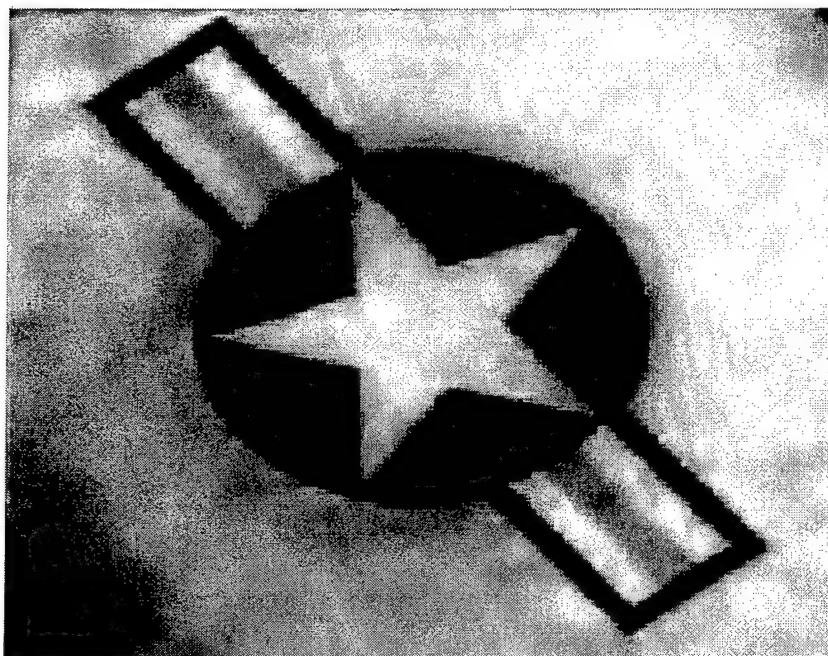


Figure 4.16: Star image denoised using (4,4) lift, 2 vanishing moments, adaptive to training signal and a soft threshold equal to 3 times the standard deviation of the noise. For entire image, $\text{PSNR} = 30.27 \text{ dB}$ and $L^\infty = 72.45$. In the training area, $\text{PSNR} = 28.12 \text{ dB}$ and $L^\infty = 59.20$.

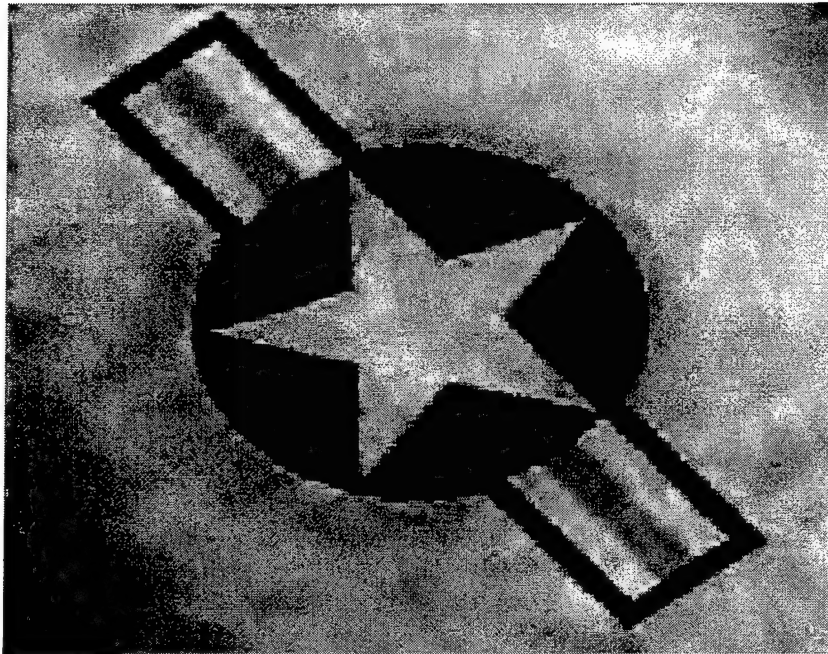


Figure 4.17: Star image denoised using (4,4) lift, 4 vanishing moments (non-adaptive) and a hard threshold equal to 3.6 times the standard deviation of the noise. For entire image, PSNR = 32.32 dB and $L^\infty = 54.04$. In the training area, PSNR = 30.22 dB and $L^\infty = 54.04$.

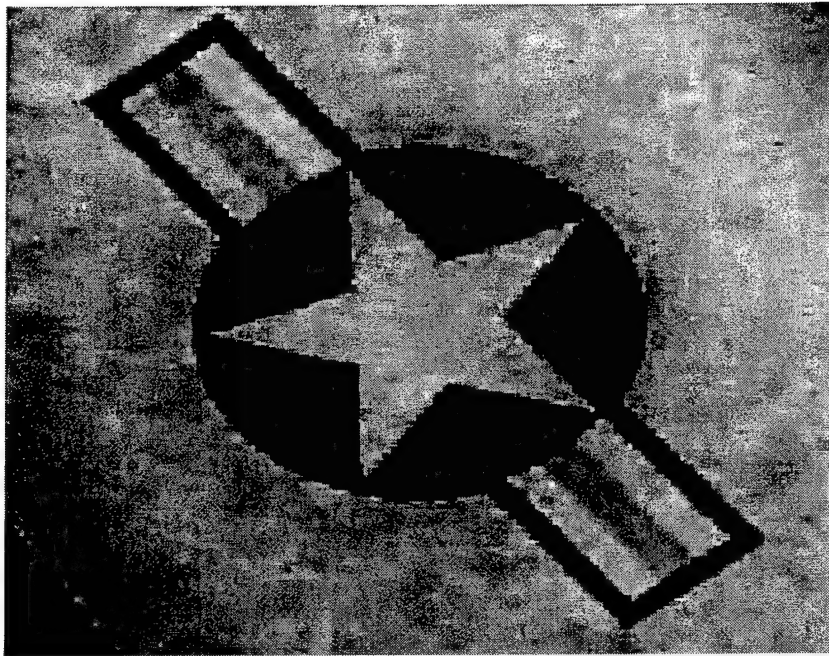


Figure 4.18: Star image denoised using (4,4) lift, 2 vanishing moments, adaptive to noisy signal and a hard threshold equal to 3.6 times the standard deviation of the noise. For entire image, PSNR = 31.93 dB and $L^\infty = 56.08$. In the training area, PSNR = 30.18 dB and $L^\infty = 56.08$.

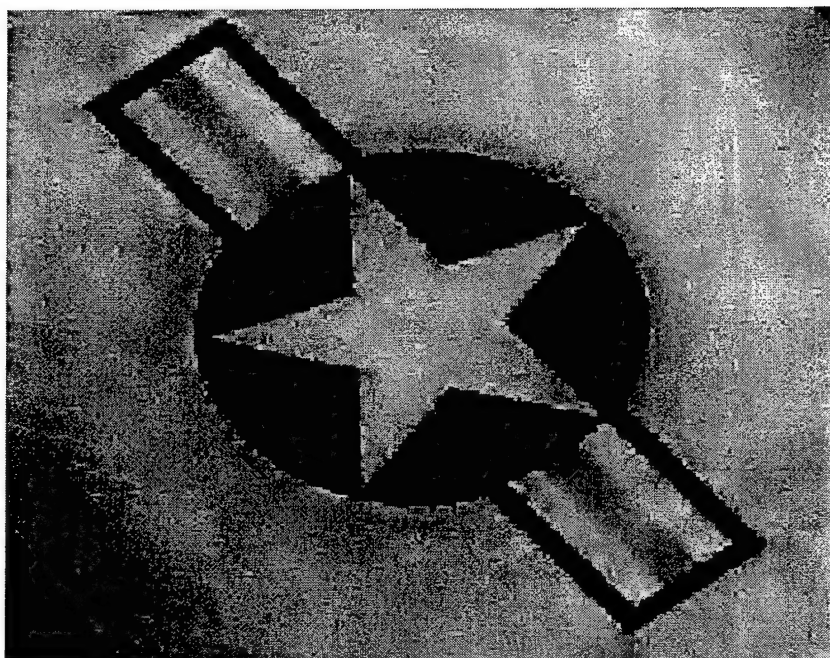


Figure 4.19: Star image denoised using (4,4) lift, 2 vanishing moments, adaptive to training signal and a hard threshold equal to 3 times the adaptive threshold set by the transform. For entire image, PSNR = 31.59 dB and $L^\infty = 52.10$. In the training area, PSNR = 30.19 dB and $L^\infty = 51.81$.

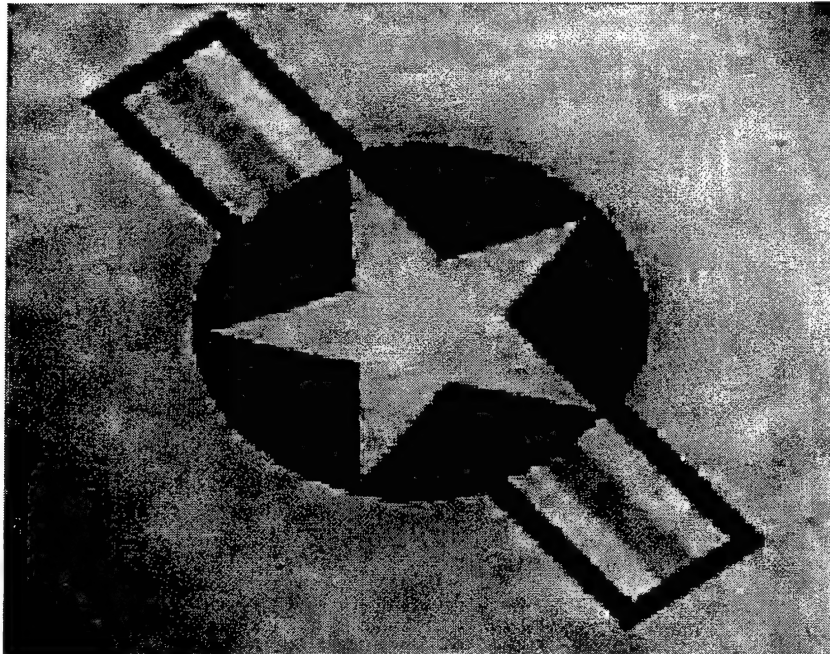


Figure 4.20: Star image denoised using (4,4) lift, 2 vanishing moments, adaptive to training signal and a hard threshold equal to 3.6 times the standard deviation of the noise. For entire image, $\text{PSNR} = 32.33 \text{ dB}$ and $L^\infty = 57.43$. In the training area, $\text{PSNR} = 30.28 \text{ dB}$ and $L^\infty = 57.43$.

Medium Noise Case PSNR (dB) measurements	Training Area of Image		Whole Image	
<div> <div></div> <div>Denoising Transform</div> </div>	Soft Threshold	Hard Threshold	Soft Threshold	Hard Threshold
Image with Noise	24.56		24.58	
(4,4) Lift 4 vanishing	27.69	30.22	29.88	32.32
(4,4) Lift 2 vanishing No training	28.81	30.18	30.91	31.93
(4,4) Lift 2 vanishing Training	28.12	30.28	30.27	32.33
(4,4) Lift 2 vanishing Training Adaptive Threshold	28.34	30.19	29.92	31.59

Table 4.3: PSNR measurements for medium noise case.

Medium Noise Case L^∞ measurements	Training Area of Image		Whole Image	
<div> <div></div> <div>Denoising Transform</div> </div>	Soft Threshold	Hard Threshold	Soft Threshold	Hard Threshold
Image with Noise	63.23		63.23	
(4,4) Lift 4 vanishing	58.83	54.04	70.87	54.04
(4,4) Lift 2 vanishing No training	55.76	56.08	66.62	56.08
(4,4) Lift 2 vanishing Training	59.20	57.43	72.45	57.43
(4,4) Lift 2 vanishing Training Adaptive Threshold	50.86	51.81	57.74	52.10

Table 4.4: L^∞ measurements for medium noise case.

4.4 Summary

The new algorithm used with the adaptive soft threshold performs very well by L^∞ measures and comparable by PSNR measures for both the whole image and the training area. The new algorithm used with the non-adaptive hard threshold gives the best overall PSNR measure, again for both the whole image and the training area. In each thresholding case, the new algorithm is better than or comparable to the (4,4) lift with 4 vanishing moments and the (4,4) lift with 2 vanishing moments adapted to the noisy signal in the PSNR and L^∞ measures.

Visually, the training algorithm results are very good. Images resulting from the training algorithms using soft-thresholds have fewer artifacts than the other images after a soft threshold was used. The adaptive threshold used with hard thresholding did not perform as well in error measures but the image is smoother with fewer artifacts than the other images after hard thresholding.

These results show that the training algorithm performs very well in the area of training and sometimes the entire image. The training algorithm obtains the best PSNR value overall the images for the whole image and the training area. The combination of the adaptive wavelets, redundancy and a priori information have proven to be useful in obtaining better image restoration.

V. Conclusion

This research explored many techniques available for image restoration and image denoising. Certain factors in the Fourier and wavelet domains still cause problems, which are visually undesirable. As technology progresses, more improvement in image restoration is desired, and can be achieved by incorporating redundancy and adaptivity into the wavelet transform. In this thesis research, a Scale Adaptive Transform (ScAT) was extended to form a redundant transform for a 2-dimensional signal. The ScAT was further modified so that it adapts to a training signal and then transforms a separate signal. In this research, the modified ScAT is trained on an image containing a priori information, typically a known object in the image. The noisy image is then transformed into the wavelet domain using the newly trained transform, where various denoising threshold techniques were applied to remove noise degradations. These techniques improved the image in the area of the known object and at times even improved the whole image. The algorithms and results presented in this thesis demonstrate that improved denoising is possible with the incorporation of redundancy and adaptivity into existing wavelet-based image restoration techniques.

5.1 Applications

An algorithm of this type could be used as a pre-processing step for many image-processing applications. In target recognition, researchers look for distinguishing features of a possible target in an image to allow a computer to locate and identify the target. An algorithm that enhances the features of the target would greatly improve the

probability of its detection in a cluttered image. This is just one example of how this type of redundant adaptive algorithm could be very useful in image restoration and image processing. In general, any image analysis application where a priori information is known about the image could be improved by the algorithms presented in this thesis.

5.2 Recommendations for Future Research

The success of this algorithm gives encouragement to continue this area of research. This technique improves noise removal in an image using redundancy, a priori information and just one adaptive prediction filter per scale; therefore, if the prediction filters also adapted spatially (e.g., multiple filters per scale), the improvement could be even greater. This modification would require developing a method to compensate with appropriate filters outside of the training area where only zeros are located (training on data comprised of all zeros is an ill-posed problem). Also, additional storage would be required for these additional prediction and update filters. This is a difficult task, due to the nature of the redundant wavelet transform. However, the creation of such a redundant spatially adaptive transform would obviously further enhance image restoration techniques.

Bibliography

- [1] R. C. Gonzalez and R. E. Woods. *Digital Image Processing*. Addison-Wesley, New York, 1992.
- [2] D. L. Donoho. "Denoising by soft-thresholding," *IEEE Trans. Inform. Theory*, vol. 41, pp. 613-627, May 1995.
- [3] C. L. Matson. "Noise reduction in images using prior knowledge as a constraint," *Proc. SPIE*, vol. 2302, pp. 36-41, Jul. 1994.
- [4] A. Chambolle, R. E. DeVore, N. Lee, and B. J. Lucier. "Nonlinear wavelet image processing: Variational problems, compression, and noise removal through wavelet shrinkage," *IEEE Trans. Image Processing*, vol. 7, pp. 319-335, Mar. 1998.
- [5] R. R. Coifman and D. L. Donoho. "Translation-Invariant De-Noising," In Anestis Antoniadis and Georges Oppenheim, editors. *Wavelets and Statistics*, pp.125-150. Springer-Verlag, New York, NY, 1995.
- [6] R. L. Claypoole, Jr. "Adaptive Wavelet Transforms via Lifting," Thesis: Doctor of Philosophy, Electrical and Computer Engineering, Rice University, Houston, Texas, Oct. 1999.
- [7] M. Belge, M. E. Kilmer, and E. L. Miller. "Wavelet domain image restoration with adaptive edge-preserving regularization," *IEEE Trans. Image Processing*, vol. 9, pp. 597-608, Apr. 2000.

- [8] I. Daubechies. *Ten Lectures on Wavelets*. CBMS-NSF Regional Conf. Series in Appl. Math., Vol. 61. Society for Industrial and Applied Mathematics, Philadelphia, PA, 1992.
- [9] W. Sweldens. The lifting scheme: A custom-design construction of biorthogonal wavelets. *Appl. Comput. Harmon. Anal.*, 3(2):186-200, 1996.
- [10] W. Sweldens. The lifting scheme: A construction of second generation wavelets. *SIAM J. Math. Anal.*, 29(2):511-546, 1997.
- [11] I. Daubechies and W. Sweldons. Factoring wavelet transforms into lifting steps. *J. Fourier Anal. Appl.*, 4(3):245-267, 1998.
- [12] H Guo, J.E. Odegard, M. Lang, R.A. Gopinath, I.W. Selesnick, and C.S. Burrus. Wavelet based speckle reduction with applications to SAR based ATD/R. *Proceedings ICIP*, Austin, TX, Nov 1994.
- [13] P. P. Vaidyanathan. *Multirate Systems and Filter Banks*. Prentice Hall, Englewood Cliffs, NJ, 1992.

Vita

Second Lieutenant Mary Kristin Marcum was born in Maryville, Tennessee. She graduated from the Heritage High School in Maryville, Tennessee. In July of 1991, she enlisted in the United States Air Force. Her first assignment was to Vance AFB, Oklahoma. She was awarded a scholarship under the SOAR program to attend the University of Tennessee at Knoxville in August of 1996. She graduated from the University of Tennessee in 1999 with a Bachelor of Science degree in Electrical Engineering. She was commissioned in May 1999 through ROTC Detachment 800 at Tennessee.

Her first duty assignment beginning in August 1999 was to attend the Air Force Institute of Technology at Wright-Patterson AFB, Ohio to earn a Masters degree in Electrical Engineering. Upon graduation in March 2001, she will report to the Air Force Research Laboratories at Kirtland Air Force Base in Albuquerque, New Mexico.

REPORT DOCUMENTATION PAGE				<i>Form Approved</i> OMB No. 074-0188	
The public reporting burden for this collection of information is estimated to average 1 hour per response, including the time for reviewing instructions, searching existing data sources, gathering and maintaining the data needed, and completing and reviewing the collection of information. Send comments regarding this burden estimate or any other aspect of the collection of information, including suggestions for reducing this burden to Department of Defense, Washington Headquarters Services, Directorate for Information Operations and Reports (0704-0188), 1215 Jefferson Davis Highway, Suite 1204, Arlington, VA 22202-4302. Respondents should be aware that notwithstanding any other provision of law, no person shall be subject to an penalty for failing to comply with a collection of information if it does not display a currently valid OMB control number.					
PLEASE DO NOT RETURN YOUR FORM TO THE ABOVE ADDRESS.					
1. REPORT DATE (DD-MM-YYYY) 07-09-2001		2. REPORT TYPE Master's Thesis		3. DATES COVERED (From - To) Jan 2000 - Mar 2001	
4. TITLE AND SUBTITLE REDUNDANT WAVELET-BASED IMAGE RESTORATION USING A PRIORI INFORMATION				5a. CONTRACT NUMBER	
				5b. GRANT NUMBER	
				5c. PROGRAM ELEMENT NUMBER	
6. AUTHOR(S) Marcum, Mary K., Second Lieutenant, USAF				5d. PROJECT NUMBER	
				5e. TASK NUMBER	
				5f. WORK UNIT NUMBER	
7. PERFORMING ORGANIZATION NAMES(S) AND ADDRESS(S) Air Force Institute of Technology Graduate School of Engineering and Management (AFIT/EN) 2950 P Street, Building 640 WPAFB OH 45433-7765				8. PERFORMING ORGANIZATION REPORT NUMBER AFIT/GE/ENG/01M-17	
9. SPONSORING/MONITORING AGENCY NAME(S) AND ADDRESS(ES) NAIC/GTN Attn: Mr. Stephen R. Hayden 4180 Watson Way Wright-Patterson AFB, OH 45433-5648 Commercial: (937) 257-7048 DSN 787-7048				10. SPONSOR/MONITOR'S ACRONYM(S)	
				11. SPONSOR/MONITOR'S REPORT NUMBER(S)	
12. DISTRIBUTION/AVAILABILITY STATEMENT APPROVED FOR PUBLIC RELEASE; DISTRIBUTION UNLIMITED.					
13. SUPPLEMENTARY NOTES					
14. ABSTRACT Reconnaissance missions and satellites collect hundreds of images loaded with valuable information to be utilized by the Air Force. Intelligence operations must analyze these images to extract the information needed to help commanders make important decisions. No matter how obtained, images of this type are often degraded by noise due to disruptions such as atmospheric disturbances, optical system variations, motion, and large distance from the sensor to the source. This noise must be removed effectively to improve the quality of these images and ensure that the information contained in them can be correctly extracted. The Air Force relies on the critical information contained in these images and therefore effective noise removal is critical. Limitations in current image restoration techniques cause visually disturbing effects in reconstructed images. Therefore, a more effective algorithm for noise removal is required. This thesis explores the use of redundant wavelet-based multiresolution image processing and a priori information to enhance current image restoration techniques. Often on an airplane, tank or other military vehicle or building there may be a known symbol, which can be used as perfect a priori information to restore the entire image. An adaptive redundant discrete wavelet transform is trained using this a priori information. Constant and adaptive thresholds are used on the noisy image while in the wavelet domain. The quality of the reconstructed image is improved over non-adaptive techniques.					
15. SUBJECT TERMS image restoration, wavelets, lifting, redundant wavelets, a priori information					
16. SECURITY CLASSIFICATION OF:			17. LIMITATION OF ABSTRACT	18. NUMBER OF PAGES	19a. NAME OF RESPONSIBLE PERSON
a. REPORT	b. ABSTRACT	c. THIS PAGE			19b. TELEPHONE NUMBER (Include area code)
U	U	U	UU	80	Maj Roger L. Claypoole, Jr., ENG (937) 255-3636, ext 4625